Paul Wilbur

NASA CR - 182255

CHARACTERIZATION OF HOLLOW CATHODE, RING CUSP DISCHARGE CHAMBERS

PREPARED FOR

LEWIS RESEARCH CENTER

NATIONAL AERONAUTICS AND SPACE ADMINISTRATION

GRANT NGR-06-002-112

by

Jason A. Vaughn

Approved by

Paul J. Wilbur

January 1989

Department of Mechanical Engineering
Colorado State University
Fort Collins, Colorado 80523

NASA
National Aeronautics and Space Administration

Report Documentation Page

1. Report No.	2. Government Accession No.	3. Recipient's Catalog No.
NASA CR - 182255		

4. Title and Subtitle
CHARACTERIZATION OF HOLLOW CATHODE, RING CUSP DISCHARGE CHAMBERS

5. Report Date
Jan. 1989

6. Performing Organization Code

7. Author(s)
Jason A. Vaughn

8. Performing Organization Report No.

10. Work Unit No.

9. Performing Organization Name and Address
Department of Mechanical Engineering
Colorado State University
Fort Collins, CO 80523

11. Contract or Grant No.
NGR-06-002-112

13. Type of Report and Period Covered

12. Sponsoring Agency Name and Address
National Aeronautics and Space Administration
Washington, D.C. 20546

14. Sponsoring Agency Code

15. Supplementary Notes Grant Monitor - Vincent K. Rawlin, NASA Lewis Research Center, Cleveland, OH 44135. This report is a reproduction of the M.S. Thesis of Jason A. Vaughn. It is submitted to the sponsor and the distribution list in this form both as a presentation of the technical material and as an indication of the academic program supported by the grant.

16. Abstract

An experimental study into the effects of changes in such physical design parameters as hollow cathode position, anode position and ring cusp magnetic field configuration and strength on discharge chamber performance, is described. The results are presented in terms of comparative plasma ion energy cost, extracted ion fraction and ion beam profile data. Such comparisons are used to demonstrate specific means by which changes in these design parameters induce changes in performance, i.e. through changes in the loss rates of primary electrons to the anode, of ions to discharge chamber walls or of ions to cathode and anode surfaces. Results show 1) the rate of primary electron loss to the anode decreases as the anode is moved downstream of the ring cusp toward the screen grid, 2) the loss rate of ions to hollow cathode surfaces are excessive if the cathode is located upstream of a point of peak magnetic flux density on the discharge chamber centerline, and 3) the fraction of the ions produced that are lost to discharge chamber walls and ring magnet surfaces is reduced by positioning the magnet rings so the plasma density is uniform over the grid surface and so there are no steep magnetic flux density gradients near the walls through which ions can be lost by Bohm diffusion. The uniformity of the plasma density at the grids can also be improved by moving the point of primary electron injection into the discharge chamber off of the chamber centerline. Other results show the discharge chamber losses decrease when a filament cathode is substituted for a hollow cathode to the extent of the hollow cathode operating power. When plasma ion energy cost is determined in such a way that the cost of operating the hollow cathode is subtracted out, the performance using either electron source is similar.

17. Key Words (Suggested by Author(s))	18. Distribution Statement
Electrostatic Ion Thruster Hollow Cathode	Unclassified - Unlimited

19. Security Classif. (of this report)	20. Security Classif. (of this page)	21. No of pages	22. Price*
Unclassified	Unclassified	84	

NASA FORM 1626 OCT 86

*For sale by the National Technical Information Service, Springfield, Virginia 22161

TABLE OF CONTENTS

Chapter		Page
I.	**INTRODUCTION**	1
	• DISCHARGE CHAMBER OPERATION	3
II.	**DISCHARGE CHAMBER PERFORMANCE MODEL**	11
	• DISCHARGE CHAMBER PERFORMANCE PARAMETERS	
	BASELINE PLASMA ION ENERGY COST (ϵ_p^*)	12
	PRIMARY ELECTRON UTILIZATION FACTOR (C_0)	14
	EXTRACTED ION FRACTION (f_B)	14
	• DETERMINATION OF PERFORMANCE PARAMETERS	15
III.	**EXPERIMENTAL APPARATUS AND PROCEDURE**	17
	• UPSTREAM FILAMENT CATHODE APPARATUS AND PROCEDURE	17
	• HOLLOW CATHODE APPARATUS AND PROCEDURE	22
	• FARADAY PROBE	29
	• MAGNETIC FIELD MAPS	30
IV.	**EXPERIMENTAL RESULTS**	35
	• THE COMPARATIVE BEHAVIOR OF REFRACTORY FILAMENT AND HOLLOW CATHODE ON PERFORMANCE	38
	• THE EFFECTS OF VARYING THE ELECTRON INJECTION REGION (CATHODE)	43
	CATHODE DIAMETER AND AXIAL POSITION (UPSTREAM OF THE RING CUSP)	43
	HOLLOW CATHODE AXIAL POSITION	50
	CATHODE DIAMETER (DOWNSTREAM OF RING CUSP)	54
	• ANODE POSITION	58
	• MAGNETIC FIELD INVESTIGATION	62
	MAGNETIC FLUX DENSITY VARIATION	62
	MAGNETIC FIELD CONFIGURATION	66
V.	**CONCLUSIONS**	74
	REFERENCES	77
	APPENDIX A: THE EFFECTS OF ION LOSSES TO CATHODE OR ANODE SURFACES ON DISCHARGE CHAMBER PERFORMANCE PARAMETERS	78

LIST OF FIGURES

Figure	Title	Page
1	Generic Discharge Chamber.	4
2	Ring Cusp Discharge Chamber with Upstream Filament Cathode	18
3	Cross Sectional View of Ring Cusp Ion Source	24
4	Typical Beam Current Density Profile	31
5a	Typical Pseudo Iron Filings Map (Computer Generated)	33
5b	Typical Magnetic Flux Density Contour Map (Computer Generated)	33
6	Typical Discharge Chamber Performance Data . .	36
7	Hollow Cathode/Filament Cathode Performance Comparison	39
8	Hollow Cathode/Filament Cathode Performance Comparison (with Keeper Potential Correction).	42
9	Effect of Upstream Filament Cathode Diameter on Plasma Ion Energy Cost Curve.	44
10	Effect of Upstream Filament Cathode Axial Position on Plasma Ion Energy Cost Curve . . .	46
11	Effects of Upstream Filament Cathode Diameter and Position on Extracted Ion Fraction	48
12	Magnetic Flux Density Contour Map (ℓ_d= 11.8 cm).	49
13	Effect of Centerline Hollow Cathode Axial Position on Discharge Chamber Performance Parameters	52
14	Centerline Magnetic Flux Density Profile . . .	55

List of Figures (continued)

Figure	Title	Page
15	Effects of Downstream Filament Cathode Diameter on Discharge Chamber Performance Parameters	57
16	Effect of Anode Position on Discharge Chamber Performance Parameters	60
17	Effect of Magnet Strength on Discharge Chamber Performance Parameters	63
18	Pseudo Iron Filings Map (B_S= 350 gauss)	65
19a	Magnetic Flux Density Contour Maps (350 gauss Surface Flux Density)	67
19b	Magnetic Flux Density Contour Map (2700 gauss Surface Flux Density)	67
20	Effect of Ring Magnet Position on Discharge Chamber Performance Parameters	69
21a	Magnetic Flux Density Contour Map (ℓ_r = 3.0 cm)	70
21b	Magnetic Flux Density Contour Map (ℓ_r = 3.6 cm)	70
22	Effect of Ring Magnet Position on Beam Flatness Parameter	72

I. INTRODUCTION

Electron bombardment ion thrusters have been identified as attractive propulsion devices for many high total impulse missions because their high specific impulse capability facilitates delivery of payloads with a mass that is a large fraction of the initial system mass. Design of progressively more efficient thrusters has, however, been impeded by a lack of understanding of the effects of changes in such design parameters as cathode and anode position on discharge chamber performance. The objective of this study is to develop a greater understanding of the mechanisms that influence discharge chamber performance. Specifically, an understanding of the means by which ring cusp magnetic field strength and configuration and the locations of the points of primary electron injection (defined by the hollow cathode position) and electron collection (defined by the anode position) relative to these fields influence discharge chamber performance.

An earlier study conducted by Hiatt [1] on a specially designed 8 cm dia ring cusp discharge chamber will be used as the starting point for this study. The study done by Hiatt concentrated on varying the point of electron collection (defined by the anode position) and seeking to understand how this affected discharge chamber performance. This study utilized a refractory filament cathode as the electron source because it facilitated ready control of the zone of primary electron injection into the discharge chamber (i.e. the field line

surface of revolution onto which primary electrons were released into the discharge chamber). Based on the results of the study by Hiatt it was concluded that the performance of a ring cusp discharge chamber is best when 1) the surface of revolution of the innermost magnetic field line that intercepts the anode (i.e. the virtual anode surface) also intercepts the outermost ring of holes in the screen grid) and 2) the surface of revolution of the outermost field line that intercepts the outer boundary of the electron source (i.e. the virtual cathode surface) is located relative to the virtual anode so that the discharge is on the threshold of extinction at the prevailing discharge voltage.

Because the more reliable, longer-lived hollow cathode class of electron sources is used in place of refractory filament cathodes in space-qualified thrusters it was desirable to conduct a study similar to Hiatt's using such cathodes and to determine how these conclusions are modified for discharge chambers equipped with hollow cathodes. This understanding was pursued in steps, with the first one involving more tests with the more convenient filament cathode to establish a starting point for the hollow cathode study. Specifically, tests were conducted to determine the general effects of the axial position of a small diameter emissive filament cathode (approximately the same diameter as that of a typical hollow cathode orifice) on discharge chamber performance. Test results from this study suggested the centerline location at which studies involving the hollow cathode should commence.

The ring cusp magnetic field was chosen as the magnetic field configuration of interest for this study because it holds substantial promise as a configuration that yields efficient discharge chamber operation [2]. The study was conducted using a small diameter

discharge chamber (~ 9 cm) which utilized high flux density magnets to produce the desired ring cusp magnetic field. Because of the small diameter of this chamber, the field lines penetrated deep into its center and this caused performance to be worse than that generally observed in larger chambers. It is noted that the performance observed in large diameter chambers could probably be realized in smaller ones if the magnetic field was adjusted so that 1) the primary electron plasma could occupy a similar fraction of the total discharge chamber volume, and 2) the magnetic flux density gradient at the chamber walls was the same. Unfortunately, a discharge chamber design that could be scaled to satisfy these two criteria simultaneously could not be found As a result the performance of the small chamber was worse than that which could be expected with a large one.

An advantage of using this small diameter discharge chamber is that the chamber performance is more sensitive to small changes in geometrical parameters than is a larger one. Because of this increased sensitivity, effects that would be undetectable in a larger diameter discharge chambers could be investigated more readily to gain the understanding of discharge chamber phenomena that is the principal goal of this research.

Discharge Chamber Operation

A cross sectional view of the essential elements of the cylindrical chamber that houses the electrical discharge between the cathode and anode in a typical ion thruster is shown as Fig. 1. The steel shell, which serves as an element of the magnetic circuit for the chamber, and the two plates (grids) through which an ion beam is extracted enclose the discharge chamber volume that is the focus of

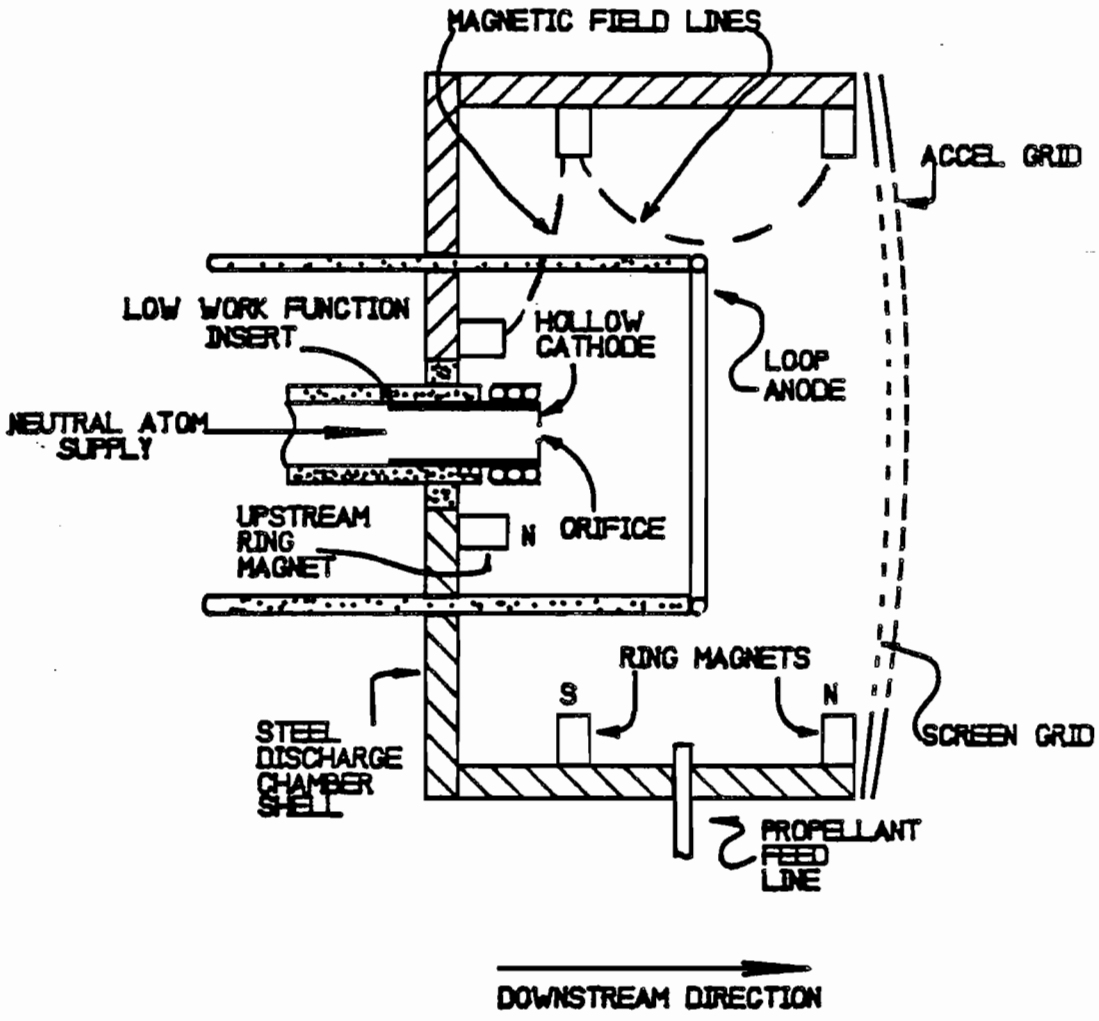

Fig. 1 Generic Discharge Chamber

this study. The two grids are uniformly spaced, dished plates that each contain a matrix of holes that are aligned in such a way that ions extracted through each hole pair tend to travel in a direction parallel to the thruster axis. The downstream plate (the accel grid) is biased negative with respect to ground and the upstream plate (the screen grid) is biased positive with respect to ground. Ions which are produced in the discharge chamber, are accelerated from the chamber by the electric field created between these two plates.

The ring cusp magnetic field shown in this figure is produced by three ring magnets, two located on the side wall of the discharge chamber and one located on the upstream surface surrounding the hollow cathode. These ring magnets are arranged with alternating polarities to produce magnetic flux lines similar to those shown in the upper half of Fig. 1. The magnetic field acts as a barrier to prevent electron losses to the anode and ion losses to discharge chamber wall, magnet and anode surfaces and cathode surfaces.

The hollow cathode shown in Fig. 1 is a device which supplies electrons into the discharge chamber [3]. It consists of a long hollow tantalum tube with a plate at one end which has a small orifice at its center. Electrons, which are emitted thermionically from a low work function surface (an insert) within this tube, collide with neutral atoms supplied within the cathode tube to create a dense plasma there. The electrons acquire the kinetic energy needed to ionize the neutral atoms by falling through an electrical potential difference sustained between insert surface and plasma and it is this same potential difference that prevents the electrons from going back to cathode or insert surfaces. Rather, the electrons generated within the cathode are drawn through the cathode orifice to the more positive discharge

chamber plasma located downstream of the orifice. The same potential difference that accelerates electrons through the orifice impedes ion flow through it so the atoms supplied into the cathode must leave as neutral atoms through the orifice. The combination of atoms and electrons escaping through the same small orifice results in additional ionization and the generation of a relatively dense plasma immediately downstream of the orifice. It is from somewhere between the cathode interior plasma and this dense downstream plasma that electrons being supplied into the discharge chamber begin accelerating to the kinetic energy they carry into the discharge plasma.

The loop anode, which defines the zone of electron collection in the discharge chamber, and the plasma immediately downstream of the hollow cathode, which defines the zone of electron emission into the discharge chamber are the two principal components that control the electron flow that is essential to operation of the discharge chamber. It is the potential difference between the discharge chamber plasma, which is near anode potential, and the plasma immediately adjacent to the hollow cathode through which ionizing (i.e. primary) electrons supplied to the discharge chamber are accelerated. The energy acquired by these electrons is, therefore, approximately equal to this potential difference.

A hollow cathode is shown as the source of electrons in Fig. 1 but a filament cathode could be used in its place. In this case the electron acceleration process would be similar, but electrons would be emitted from the filament surface directly into the discharge chamber plasma. The energy acquired by these primary electrons would be approximately equal to the full cathode-to-anode potential difference (the discharge voltage - V_D). Because primary electrons emitted from

a hollow cathode originate from a plasma immediately adjacent to it and because this plasma is always at a potential above that of the cathode surface, the energy they obtain is equal to the discharge voltage minus the cathode-to-cathode plasma potential difference. The energy of the primary electrons drawn from a filament cathode is therefore greater than the energy of primary electrons drawn from a hollow cathode in thrusters where the discharge voltage is the same. It is believed that most of the primary electron energy deficit for the hollow cathode case goes into sustaining the operation of the hollow cathode.

Primary electrons, which are emitted from the hollow cathode shown in Fig. 1, travel along magnetic field lines (through the ambipolar diffusion process [4]), which pass close to the hollow cathode orifice, with relative ease. These electrons can ionize neutral atoms that have been introduced into the discharge chamber as propellant and find themselves near these magnetic field lines. In order for electrons to reach atoms in other regions of the discharge chamber they must migrate across rather than along magnetic field lines. This process is facilitated by momentum transfer collisions which can occur between primary electrons and the other particles in the discharge chamber. As primary electrons have both momentum transfer and inelastic (ionization and excitation) collisions they tend in general to both lose energy and diffuse toward the anode where they can be collected and removed from the discharge chamber. The lower energy electrons which have had inelastic collisions and those electrons which are a product of the ionizing collisions fall into a near-Maxwellian distribution and these electrons exhibit a greater probability for subsequent momentum transfer collisions than do primary electrons (collision frequency increases as electron energy decreases). Because of this effect and

the fact that electrons migrate along field lines with relative ease, the migration of lower energy electrons from the field lines passing near the cathode to those passing near the anode is facilitated. This is fortunate because it causes the lower energy electrons that have given up much of their energy to be collected in preference to high energy (primary) electrons. The loss rate of both primary and Maxwellian electrons to the anode times their charge is the discharge current (J_D). The product of this current and the potential difference through which the primary electrons are accelerated represents the power being supplied to the discharge chamber.

The primary electrons which do not have inelastic collisions gyrate around in the discharge chamber until they are collected by the anode. When a primary electron is collected by the anode before it has had an inelastic collision, its energy is lost to the anode. For the discharge chamber to operate efficiently the number of primary electrons being lost to the anode without such collisions must be minimized.

The preceeding discussion has addressed some features of the process of electron migration in a discharge chamber, but it has not suggested how ions might migrate. In reality both the ions and the electrons tend to undergo gross migration together in an effort to prevent charge separation between the two species [4]. The eventual fate of the ions is not as definite as that for the anode bound electrons. Ions can be lost to the magnet rings, to the discharge chamber surfaces or into the beam. The two phenomena that have a dominant influence on where the ions are lost from the discharge chamber are associated with plasma diffusion along and across magnetic field lines. The diffusion of ions and electrons along field lines

(ambipolar diffusion) is not dependent on the magnetic flux density. The rate of diffusion across field lines (Bohm diffusion) on the other hand depends inversely on the magnetic flux density in the region of the chamber where the diffusion rate is being computed. Hence the more intense the magnetic field (higher flux density) the smaller the ion loss rate across the associated magnetic field lines.

Energy is supplied to the discharge chamber by the primary electrons only, but it is removed from the plasma by the ion and electron loss mechanisms that have been described. The primary electron energy which was expended during the collisional process to produce an ion, is also lost when these ions go to the various surfaces in the discharge chamber. Also, energy is lost from the plasma by collection of primary and Maxwellian electron energy at the anode. These energy loss mechanisms all tend to degrade discharge chamber performance.

Discharge chamber performance measurements are made in terms of the energy that is supplied to produce an ion which is extracted into the beam (designated ϵ_B- the beam ion energy cost) and the fraction of the total neutral atoms being supplied as propellant that are extracted into the beam as ions (designated η_u- the propellant utilization efficiency). These measurements indirectly take into account the energy being lost to the anode by the collection of both primary and Maxwellian electrons and the loss of ions to discharge chamber and magnet surfaces. However, because all energy loss mechanisms are included in just these two terms, it is difficult to determine exactly which energy loss mechanism is causing a particular change in performance. A method which describes discharge chamber performance in more detail and reflects changes in the loss rate of electrons to the

anode or ions to discharge chamber surfaces independent of one another is needed if increased understanding of ion thruster operation is to be realized. Such a method is described in the next chapter.

II. DISCHARGE CHAMBER PERFORMANCE MODEL

A model developed by Brophy [5] summarized by a simple algebraic equation has been used to describe discharge chamber performance. This equation, which describes the variation of beam ion energy cost (ϵ_B) as a function of propellant utilization efficiency (η_u) in terms of physically meaningful parameters which can be related to ion and electron loss rate phenomena, is shown in Eq. 1.

$$\epsilon_B = \frac{\epsilon_P^*(1 - \exp[-C_0\dot{m}(1 - \eta_u)])^{-1}}{f_B} + \frac{(1 - f_B)V_D}{f_B} \qquad (1)$$

Five parameters which appear in this equation must be defined before it can be used to describe discharge chamber performance i.e. define the curve of ϵ_B vs. η_u. Two of these parameters, the discharge voltage (V_D) and propellant mass flowrate ($\dot{m}$), are set by the designer or ion thruster operator to assure operation for an acceptable discharge chamber lifetime at an specified thrust level so they may be considered free parameters for the purposes of this work. The three remaining parameters the baseline plasma ion energy cost (ϵ_P^*), the primary electron utilization factor (C_0), and the extracted ion fraction (f_B) describe the energy lost from the plasma by the primary and Maxwellian electrons collected by the anode and ions lost to various discharge chamber surfaces. These parameters are also dependent on discharge voltage, propellant type and the potential of the plasma immediately

downstream of the hollow cathode orifice from which primary electrons are supplied to the discharge chamber. The three parameters will be referred to as the discharge chamber performance parameters throughout this study because a knowledge of their values is all that is required to describe discharge chamber performance and identify the rate of ion and electron losses to discharge chamber and anode surfaces for a chamber operating on a prescribed propellant at a prescribed discharge voltage with a known primary electron source potential.

The first term in Eq. (1) represents the energy cost (or average energy supply requirement per beam ion) for producing ions in the discharge chamber and then extracting a fraction (f_B) of them into the beam and the second term represents the energy cost of accelerating ions into discharge chamber surfaces. Examination of Eq. (1) suggests that performance is improved by decreasing the baseline plasma ion energy cost, increasing the primary electron utilization factor and increasing the extracted ion fraction. It is noted that all of these parameters have been shown to be independent of propellant flowrate [5]. Because of this the test procedures are simplified and it is possible to determine values of each of these parameters using data collected over a large range of flowrates.

Discharge Chamber Performance Parameters

Baseline Plasma Ion Energy Cost (ϵ_p^*)

The baseline plasma ion energy cost (ϵ_p^*) is a measure of the energy required to produce ions in the discharge chamber when the neutral atom density is sufficiently high so that all primary electrons undergo inelastic collisions and fall into the Maxwellian electron group before they reach the anode and are collected. Ideally,

the value of baseline plasma ion energy cost would be equal to the ionization potential of the particular atom being used as propellant because it represents the energy that a primary electron will lose when it ionizes an atom. Because unavoidable energy losses are occurring during the ionization process, however, the ideal case is never observed. The unavoidable energy losses that occur result from the collection of Maxwellian electrons at the anode, the inelastic collisions of primary electrons with neutral atoms that produce excited rather than ionized state atoms, and the energy to operate the hollow cathode if one is being used. For the purposes of this study the energy losses associated with excitation collisions and the operation of the hollow cathode can be considered constant. One would expect, therefore, recognizing that the average energy of Maxwellian electrons collected at the anode is typically relatively invariant, that the baseline plasma ion energy cost would be relatively constant. There is, however, an experimental effect that prevents realization of this expectation.

This experimental effect reflects the fact that ions produced in the discharge chamber are lost to the cathode and anode surfaces and the currents of these ions are both small compared to the electron current going to and coming from these surfaces and indistinguishable from electrons coming from and going to the same surfaces. Therefore, the current of ions which are going to the cathode (electron emission zone) and the anode (electron collection zone) cannot be correctly measured. When a significant fraction of the ions produced in the discharge chamber is being lost to one of these surfaces, a noticeable increase in ϵ_p^* is observed. An increase in this parameter is therefore interpreted as an increase in ion losses to one of these surfaces.

Primary Electron Utilization Factor (C_0)

The primary electron utilization factor (C_0) describes the probability that a primary electron coming from the cathode will have an inelastic collision and lose energy before reaching the anode. This parameter accounts for the primary electron energy that is being removed from the plasma by the direct loss of primary electrons to the anode. Imbedded in this parameter is the distance a primary electron travels before reaching the anode if it has no inelastic collisions (ℓ^* - the primary electron containment length). When ℓ^* is increased (by applying a magnetic field to limit electron motion toward the anode for example) the probability that an primary electron will have an inelastic collision is increased. The value of the parameter ℓ^* depends not only on the magnetic field, but also on the thruster geometry and the relative positions of the anode and cathode.

The primary electron utilization factor also depends on the propellant type and the quality of neutral atom containment by the grids. During the conduct of comparative experiments effort was made to hold these parameters constant so that variations observed in C_0 may be considered to reflect proportional changes in ℓ^*.

Extracted Ion Fraction (f_B)

The extracted ion fraction (f_B) represents the fraction of the total ions produced in the discharge that are extracted into the beam. This factor accounts for the loss of energy expended by electrons to make ions that are being lost to discharge chamber surfaces and are not contributing to the ion beam current. Indirectly, this factor provides an indication of how well the magnetic field is confining and directing ions toward the grid system.

Determination of Performance Parameters

Values of the three performance parameters (ϵ_P^*, C_0 and f_B) can be calculated from the raw data collected during experiments. This is accomplished by first measuring the currents and the voltage needed to determine the energy required to produce an ion in the plasma (plasma ion energy cost (ϵ_P)) as a function of propellant flowrate ($\dot{m}$) and propellant utilization efficiency (η_u) as well as the extracted ion fraction (f_B). The extracted ion fraction can be computed directly from the data, but some manipulation of the data is required before the other two parameters can be determined. This is accomplished by computing the plasma ion energy cost (ϵ_P) and the neutral density parameter
($\dot{m}[1 - \eta_u]$) from the data and then plotting these parameters against each other. It is noted that the neutral density parameter ($\dot{m}[1 - \eta_u]$) derives its names from the fact that it is the loss rate of neutral atoms through the grids and is proportional to the atomic density in the discharge chamber [5]. Once the ϵ_P vs. ($\dot{m}[1 - \eta_u]$) plot has been generated the data in it are fitted using the equation for plasma ion energy cost developed by Brophy [5], imbeded in Eq. 1 and shown below.

$$\epsilon_P = \epsilon_P^* \left(1 - \exp[-C_0 \dot{m}(1 - \eta_u)]\right)^{-1} \qquad (2)$$

Specific values of ϵ_P^* and C_0 associated with a particular set of data are obtained by finding the best fit of Eq. (2) to them using a non-linear least-squares curve fit technique. Thus, discharge chamber performance can be determined by measuring plasma ion energy cost and extracted ion fraction data during a typical experiment. A detailed description of the measurement and calculation techniques used to determine plasma ion energy cost as a function of neutral density

parameter and to compute corresponding extracted ion fraction data is presented in the Apparatus and Procedure section of this thesis.

III. EXPERIMENTAL APPARATUS AND PROCEDURE

Upstream Filament Cathode Test Apparatus and Procedure

The ring cusp discharge chamber used to investigate the effects of the position and diameter of a refractory metal filament cathode located upstream of the ring magnet on discharge chamber performance is shown in Fig. 2. This figure shows a cross sectional view of the steel discharge chamber which for these tests had a diameter and length (ℓ_d) that were held constant at 9 cm and 11.8 cm, respectively and which utilized a grid set that was masked down to produce an ion beam with a diameter (d_b) of 8.0 cm. The test apparatus shown was designed as research tool in which all the geometrical lengths labeled in Fig. 2 could be adjusted from one test to the next. The axial position of the single radially facing ring magnet on the chamber wall and the discharge chamber length (ℓ_r and ℓ_d) are measured with respect to the screen grid plane while the position of the loop anode and the filament cathode (ℓ_a and ℓ_c) are measured with respect to the axial reference location at the center of the ring cusp electrode. Negative values of both ℓ_a and ℓ_c represent anode and cathode positions which are upstream of the reference location.

The ring cusp magnetic field in this discharge chamber is induced by a single ring magnet facing radially into the chamber and a single magnet on the upstream surface of the discharge chamber. The magnet ring and the single upstream magnet were made up of 1.9 cm by 1.3 cm by 0.5 cm samarium cobalt magnets with a surface flux density of

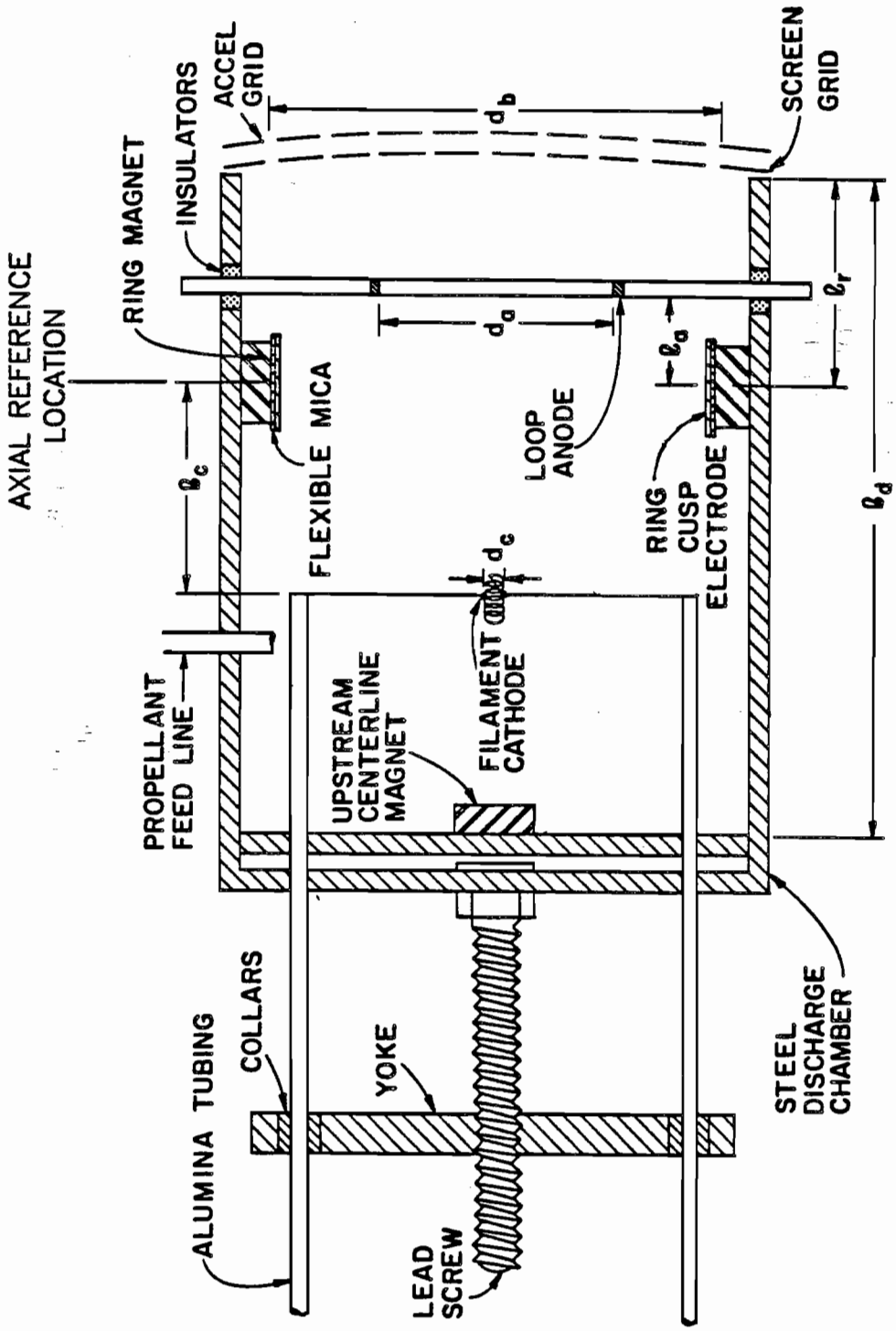

Fig. 2 Ring Cusp Discharge Chamber with Upstream Filament Cathode

0.27 Tesla. The ring magnet was constructed by placing individual magnets end-to-end around the inner circumference of the chamber while a single magnet placed at the center of the upstream surface served as the upstream centerline magnet. The ring and upstream centerline magnets were arranged with their outward facing surfaces opposite in polarity from each other to produce the desired field.

The filament cathode shown in Fig. 2 was constructed by coiling 0.025 cm dia tungsten wire into a helix with a major diameter d_c and its axis coincident with the discharge chamber centerline. The diameter of the filament was varied by increasing or decreasing the number of coils in a constant length of wire to produce the desired diameter. The largest filament cathode had only a single winding while the smallest filament cathode had numerous windings. Under the action of the lead screw and yoke the filament cathode position (ℓ_c) could be varied from the axial reference location to a point a few centimeters downstream of the upstream end while the device was operating.

Two anodes were available for use during the conduct of the tests; the loop anode shown in Fig. 2 had its center coincident with the discharge chamber centerline and had a diameter d_a. The other anode was located on the ring magnet surface, and because it could be biased either positive and negative of the cathode to serve as either an anode or an ion collection surface it is designated as a ring cusp electrode in Fig. 2. The ring cusp electrode was made of 0.025 cm thick stainless steel placed directly over the ring magnet and a layer of flexible mica was placed between the electrode and the ring magnet surface to isolate the electrode from the discharge chamber walls. The ring cusp electrode was held in place by spot welding small steel strips to the stainless steel between the surface of the magnet and the

electrode. The loop anode which was made of copper was fixed axially 1.7 cm downstream of the ring cusp position but its diameter (d_a) could be varied if desired. The ring cusp electrode and loop anode were connected electrically so that both or either could be switched from anode potential.

During the course of the experiments it was found that a discharge could not be sustained using the loop anode alone. Also, when the loop and ring cusp anodes were used together test results were found to be no different than those obtained using the ring cusp anode alone [6]. This suggests that the ring cusp anode controls discharge chamber performance when it is present. Therefore, all results presented will involve operation with the ring cusp anode alone.

The dished small hole accelerator grid (SHAG) optics set used in all tests has screen and accel hole diameters of 1.9 mm and 1.5 mm, respectively, and these holes are arranged with a 2.2 mm centerline to centerline spacing. The cold grid spacing was 0.6 mm and the grids were maintained at 750 V (screen grid) and -250 V (accel grid) for all tests. The experiments were conducted in a 46 cm dia bell jar which was diffusion pumped to a background pressure in the low 10^{-6} Torr range. Typical operating pressures were in the high 10^{-4} Torr range over the range of argon flowrates used in the tests.

The basic test procedure involved establishing an argon flowrate of 500 mA eq and starting a discharge by heating the cathode filament and applying a discharge voltage of 50 V. Initially, the flowrate was set at a desired operating condition and the total mass flowrate ($\dot{m}_T$ expressed in mA eq) and the discharge chamber background pressure (P_o) were measured. When operation had stabilized, the discharge current (J_D) was varied in increments over a range of 0.2 A to 1.5 A. At each

discharge current condition the discharge current, beam current (J_B), and total ion production (J_P) expressed as a current were measured. This latter current was measured by biasing the discharge chamber walls, magnets and the screen grid 30 V negative of the hollow cathode to repel all electrons from these surfaces so the ion current reaching each of them could be sensed. The discharge chamber magnet and wall current (J_W), the screen grid current (J_S) and the beam current were all measured separately and then summed to obtain the total ion production current.

$$J_P = J_W + J_S + J_B \tag{3}$$

With the total ion production current known, the plasma ion energy cost (ϵ_P- the energy cost of producing an ion in the plasma) and the extracted ion fraction (f_B- the fraction of the total ions produced in the discharge chamber being extracted into the beam) could be computed using the expressions [1,5]

$$\epsilon_P = \frac{V_D(J_D - J_P)}{J_P} \tag{4}$$

and,

$$f_B = \frac{J_B}{J_P} \quad . \tag{5}$$

The neutral density parameter ($\dot{m}[1 - \eta_u]$) was computed using

$$\dot{m}(1 - \eta_u) = \dot{m}_T + \frac{P_o A_b \phi_o e}{\sqrt{2\pi m_i k T_o}} - J_B. \tag{6}$$

The second term on the right hand side of this equation accounts for neutral atom backflow through the grids. It can be computed because the beam area (A_b), the transparency of the grids to neutral atom back flow (ϕ_o), the atom/ion mass (m_i), Boltzmann's constant (k), and the electronic charge (e) are all known. The ambient (vacuum chamber) neutral atom temperature (T_o) is assumed to be 300 K and the vacuum chamber pressure (P_o) is measured at each operating condition.

When all necessary data at one particular flowrate had been recorded, the flowrate was increased so performance data could be collected over the neutral atom density range of interest. For this particular test sequence that range was typically 200 to 500 mA eq. After the flow conditions of interest had been investigated, the filament cathode was repositioned and data similar to that just described were recorded. In conducting the study the cathode was moved from the location of the ring cusp (ℓ_c = 0 cm) to just downstream of the upstream discharge chamber surface (ℓ_c = -2.5 cm). After the entire range of positions had been investigated the cathode filament diameter (d_c) was changed by manually removing the discharge chamber from the vacuum system and changing the filament. The discharge chamber was reinstalled and the test procedure just outlined was repeated over a similar range of argon flowrates and cathode positions. The cathode diameter (d_c) was varied from 0.2 cm to 3.2 cm in the conduct of these tests.

Hollow Cathode Test Apparatus and Procedure

The test apparatus for the tests, which involved the use of the hollow cathode electron source, is shown in Fig. 3. This figure shows a cross-sectional view of the test apparatus which is very similar to

the discharge chamber equipped with the upstream filament cathode. The differences in the two pieces of test apparatus were made principally to facilitate use of the hollow cathode. The chamber was shortened to 5 cm so the cathode could be positioned both upstream and downstream of the axial reference location at the ring cusp. An extra ring magnet was added near screen grid to reduce the extent to which stray magnetic field lines extend toward the center of this shorter discharge chamber. The beam diameter (d_b) was reduced to 7.0 cm because the ring magnet near the screen grid protruded into an 8 cm dia beam. Finally, the loop anode was made movable so it could be positioned to induce stable operation of the discharge at a desired discharge voltage level.

The ring cusp magnetic field in this discharge chamber was produced by two radially facing ring magnets with their mid lines located 0.3 cm and ~3.0 cm upstream of the screen grid and one axially facing ring magnet surrounding the hollow cathode and located on the upstream end of the discharge chamber. The axial position of the central ring magnet, which is located a distance ℓ_r upstream of the grids, was varied during one test, but the ring magnet nearest the screen grid and the one on the upstream face remained fixed throughout all tests. Note that the positions of the anode (ℓ_a) and cathode (ℓ_c) are measured with respect to the axial reference location at the center of the central (radially facing) ring magnet and negative or positive values of ℓ_a or ℓ_c indicate respectively upstream and downstream positions of the anode or hollow cathode. Each ring magnet is made up of small (1.2 cm by 0.6 cm by 0.5 cm) samarium cobalt magnet segments with a strength of 0.27 T at their surfaces. The rings were formed by placing the magnet segments end-to-end around the inner circumference of the discharge chamber (radially facing magnets) and in a circular

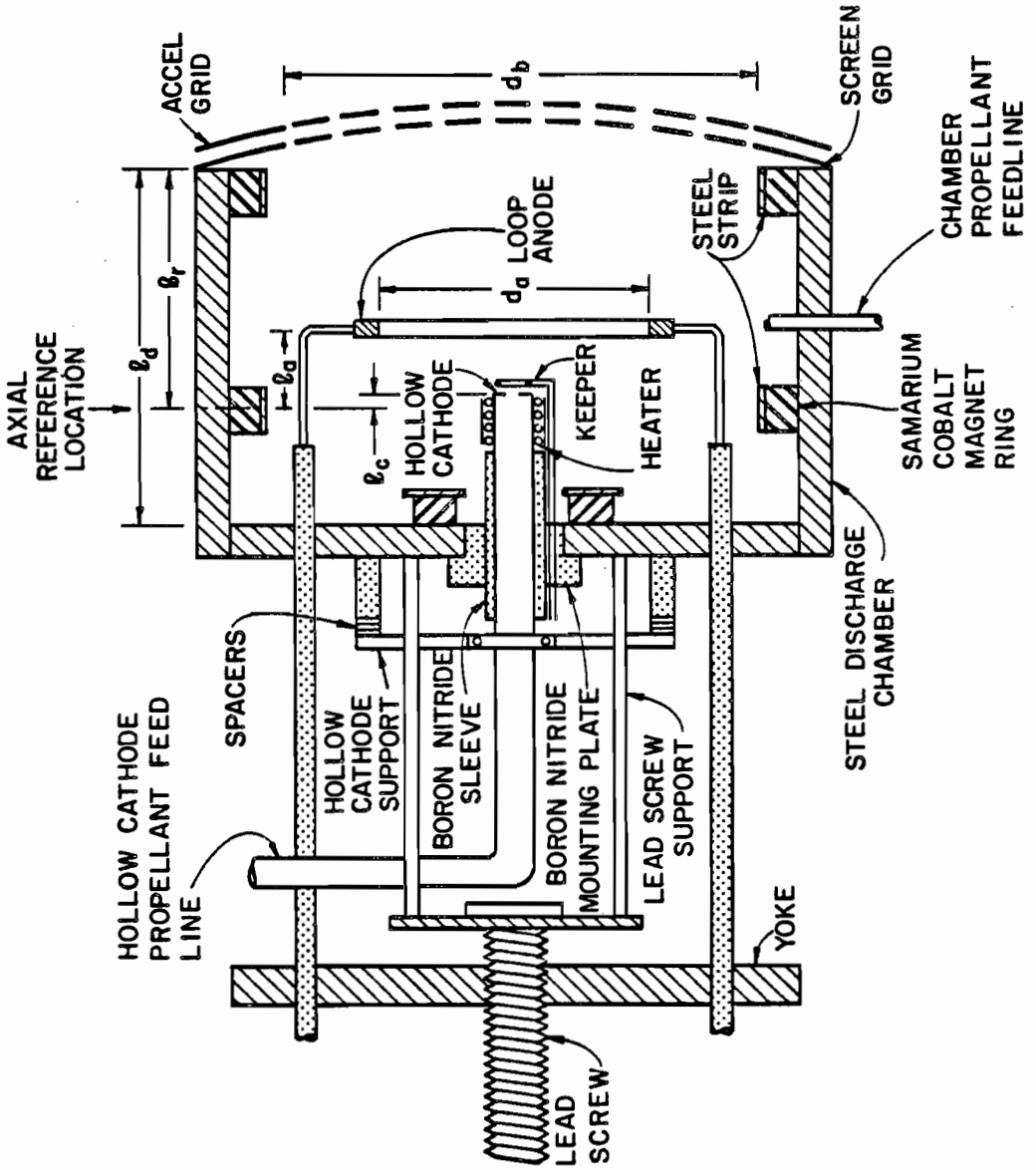

Fig. 3 Cross Sectional View of Ring Cusp Ion Source

pattern with an approximate diameter of 3.0 cm (upstream magnet). The steel strips and the washer, which are shown covering the radial and axially facing magnets respectively in Fig. 3, were used to distribute the magnetic flux uniformly over each ring surface during tests in which the numbers of magnet segments in each ring were varied and the effects of magnetic flux density on discharge chamber performance were investigated.

The tantalum loop anode shown in Fig. 3 is designed so the center of the anode moved coincident with the discharge chamber centerline. The loop anode has a fixed diameter (d_a) of 5.2 cm and under the action of the lead screw and yoke it can be moved either upstream or downstream of the axial reference location. Because anode locations upstream of the reference location resulted in very poor performance and instabilities that prevented data collection, results pertaining only to downstream anode locations (positive values of ℓ_a) will be presented.

A 0.64 cm dia tantalum tube that was electron beam welded to a tungsten orifice plate with a 0.76 mm dia orifice served as the hollow cathode shown in Fig. 3. It utilized an R-500* treated rolled tantalum foil insert and was equipped with a swaged heater to facilitate startup. As the figure suggests the cathode is mounted in an electrically insulating boron nitride mounting plate-sleeve assembly, which keeps it isolated electrically but allows it to be moved axially from one test to the next by changing spacers at the

---

* Chemical R-500 is a double carbonate ($BaCO_3$, $SrCO_3$) mixture that has been manufactured by the J.R. Baker Chemical Co., Phillipsburg, N.J. but is no longer made.

cathode supports. This assembly is sufficiently leak tight to prevent significant propellant leakage from the discharge chamber into the vacuum system. The cathode orifice plate can be moved upstream (negative ℓ_c) and downstream (positive ℓ_c) of the axial reference location. The toroidal tantalum keeper shown in Fig. 3 has a 0.16 cm minor diameter and a 0.32 cm major diameter, is positioned 0.8 mm downstream of the hollow cathode orifice plate and is supported by the boron nitride mounting plate.

Xenon propellant was used in all of the hollow cathode discharge chamber tests because it facilitated operation at low cathode flowrates and simplified the conduct of the tests. It was supplied through both the hollow cathode (at a flowrate - $\dot{m}_c$) and the main propellant feed line (at a flowrate - $\dot{m}_d$). The total flowrate ($\dot{m}_T$) into the chamber, used to compute the neutral density parameter ($\dot{m}[1 - \eta_u]$- see Eq. (6)), reflected both of these measured flows as well as the computed neutral atom backflow from the chamber through the grids described in Eq. (6).

$$\dot{m}_T = \dot{m}_c + \dot{m}_d \qquad (7)$$

Typical vacuum chamber background operating pressures using xenon propellant were in the high 10^{-5} to low 10^{-4} Torr range.

Experimental tests were initiated by flooding the hot hollow cathode with xenon propellant and then applying a sufficiently high keeper voltage (~200 V) to start a keeper discharge. After startup the keeper voltage was varied as required to maintain a 0.1 A keeper current for all testing. The cathode flowrate was reduced once the keeper discharge had started and a discharge to the anode, which was held at a potential 40 V above cathode potential, was established. The

current being drawn to the anode was maintained at approximately an ampere by controlling the main and/or cathode flowrates until thruster operation had stabilized. After a period of stabilization, tests were typically conducted by setting the xenon flowrate through the hollow cathode to ~ 20 mA eq (Xe) and that into the discharge chamber to ~ 95 mA eq (Xe) while maintaining the discharge voltage (V_D) at 40 V. The cathode and discharge chamber flowrates ($\dot{m}_c$ and $\dot{m}_d$), the vacuum chamber background pressure (P_o), the keeper voltage (V_k), the discharge current (J_D), beam current (J_B), and total ion production rate expressed as a current (J_P), corresponding to this operating condition were all measured and recorded. The total ion production rate associated with each operating condition was computed from ion currents measured in the same way as that described for the upstream filament cathode (Eq. 3). These data were used in Eqs. 4, 5, 6 to calculate the plasma ion energy cost (ϵ_P), the extracted ion fraction (f_B), and the neutral density parameter ($\dot{m}[1 - \eta_u]$).

After all the currents (J_D, J_B and J_P), the voltage (V_k) and other data had been recorded at the initial flow condition, the discharge chamber flowrate was increased while the hollow cathode flowrate and discharge voltage were held constant. This caused the discharge current and hence the other currents and keeper voltage to change and their new values were recorded. This process of increasing discharge chamber flowrate and recording data was continued until the accel grid impingement current increased to ~10 mA. The hollow cathode and discharge chamber flowrates were then both reduced and the process of recording data, as the discharge chamber flowrate was increased incrementally and the cathode flowrate and discharge voltage were held constant, was continued. This process of reducing the hollow cathode

flowrate and increasing the discharge chamber flowrate incrementally continued until data had been recorded over a wide range of discharge chamber neutral atom density levels (and therefore a wide range of discharge currents) at the prescribed 40 V discharge voltage. Typically, the hollow cathode flowrate ($\dot{m}_c$) had to be decreased from 20 to 10 mA eq (Xe) while the discharge chamber flowrate ($\dot{m}_d$) had to be increased from 95 to 460 mA eq (Xe) to cover an adequate range of neutral atom densities.

The effects of varying the position of the anode and the hollow cathode were investigated by first placing the cathode at a particular location in the discharge chamber and then moving the anode downstream in increments (i.e. onto field lines located progressively further from the field lines intersecting the hollow cathode orifice). At each anode position, plasma ion energy cost and extracted ion fraction data were recorded as a function of neutral density parameter using the procedure described in the preceeding paragraph. This process continued until the anode was so far downstream of the cathode that the discharge currents drawn to the anode were small. The cathode was then repositioned and the process of moving the anode and varying the flowrates was repeated. The range of cathode positions investigated was from 0.6 cm upstream (ℓ_c= -0.6 cm) to 0.5 cm downstream (ℓ_c= 0.5 cm) of the reference location.

A second set of experiments was conducted in which the effects of varying the magnetic flux density (B_S) at the surfaces of both the steel strips and the washer covering the ring magnets was investigated. The magnetic flux density was varied by removing individual samarium cobalt magnet segments from each ring magnet and placing a steel strip or washer of sufficient thickness to produce a common, uniform surface

magnetic flux density over the entire surface of each ring magnet. This required that the thickness of the strips and the washer be increased as the surface magnetic flux density was decreased in increments from 2700 gauss to 350 gauss. At each magnetic flux density condition plasma ion energy cost and extracted ion fraction data were recorded as a function of discharge chamber neutral density parameter using the experimental procedure described previously.

A final experiment was conducted in which the upstream ring magnet position (ℓ_r) was varied from 2.7 to 3.6 cm in increments of 0.3 cm to determine the effects of such changes on discharge chamber performance. The positions of the anode and hollow cathode were held constant relative to the reference location on this magnet during the test, so magnet ring, anode and cathode were all moved in unison. The procedures used to measure plasma ion energy cost data as a function of discharge chamber neutral density parameter were as described previously.

Faraday Probe

A Faraday probe, which is a device that measures the current of ions on a small collector (operation is described by Huddlestone [7]), was used to measure beam current density profiles. These beam current density profiles when analyzed provide insight into the effects that geometrical changes inside the discharge chamber have on the distribution of ions at the ion extraction grids and therefore on the distribution of ion current density across a grid system diameter.

The Faraday probe used in this study consists of a 0.6 cm dia molybdenum ion current sensing disc that is shielded from the beam plasma electrons by a stainless steel screen biased 9 V below ground

potential and is enclosed in a stainless steel body. The Faraday probe was located 4 cm downstream of the screen grid for this particular study. Figure 4 shows a typical beam current density profile; this one was measured at a 100 mA beam current (J_B) and the other conditions defined in the legend (see Fig. 3) by simultaneously inputing signals proportional to the ion current being collected by the probe sensor and the radial position of the probe to an x-y recorder.

The beam current density profiles were analyzed numerically to determine the beam flatness parameter and total beam current (i.e., the integrated beam current) associated with the profile. Integrated beam currents were always found to agree with directly measured beam currents to within ± 10 %. The beam flatness parameter is a measure of the uniformity of the beam profile and is defined as the average-to-maximum beam current density ratio measured near the grids.

Magnetic Field Maps

The magnetic field configuration in a discharge chamber has a major influence on discharge chamber performance and a map of the magnetic field provides visual information that can be used to show how the plasma distributes itself in a chamber and where ions and electrons will be lost to various surfaces through the mechanisms of ambipolar and Bohm diffusion. Two specific maps (iron filings and magnetic flux density contour maps) provide useful information in this application. An iron filings map is a physical picture of a magnetic field obtained when iron filings placed on a surface in a magnetic field are allowed to align along field lines and then frozen in place [8]. This type of map is useful because it enables one to see where electrons can move readily (i.e. along field lines by the mechanism of ambipolar

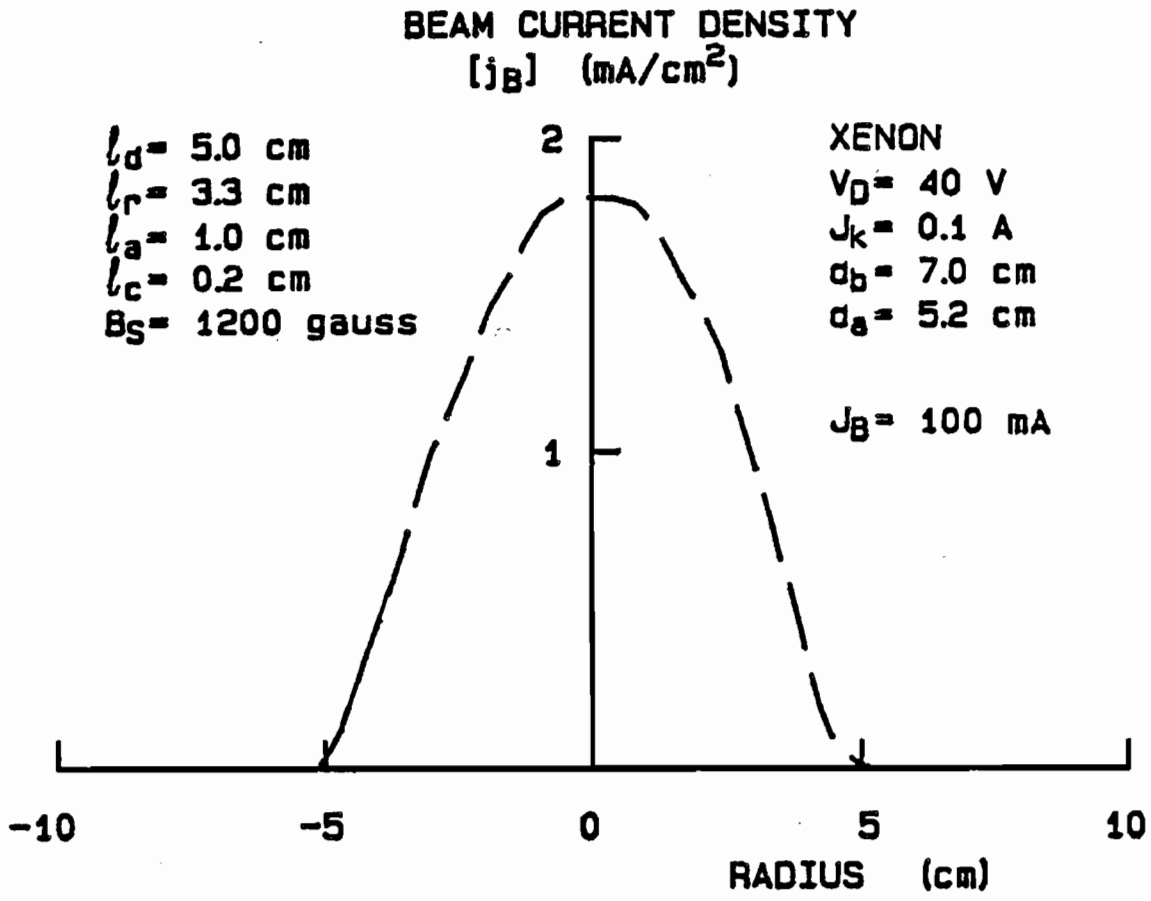

Fig. 4 Typical Beam Current Density Profile

diffusion). A magnetic flux density contour map on the other hand is constructed by measuring magnetic flux densities throughout a chamber and then joining points of constant magnetic flux density superimposed on an outline of the chamber. This map can be used to help identify zones of high magnetic flux density gradient in the discharge chamber where ions are likely to reach discharge chamber boundaries (by the mechanism of Bohm diffusion).

Both iron filings and magnetic flux density contour maps are useful in determining why a particular chamber configuration exhibits good or bad performance but they are time consuming to make. A computer algorithm developed by Arakawa [9] can, however, be used to make them numerically by simply defining geometrical and magnetic property information to the code. The computer algorithm allows the user to enter parameters which describe the discharge chamber geometry, the permanent magnet locations in the discharge chamber and their magnetization levels. The program then generates a finite element mesh and solves for the magnetic field vector potential at each element using the finite element method. The magnetic field vector potential can be plotted as a function of position in the discharge chamber to produce a computer-generated (pseudo) iron filings map like the one shown in Fig. 5a. This particular map was produced for a flux density measured at the surface of the steel strips (B_S) of 1200 gauss and the geometric data shown in the legend (symbols are defined in Fig. 3). Because the computer program generates an axis-symmetric view, only half of the map is plotted. By taking the gradient of the vector potential map the program can also be used to generate a constant flux density contour map. Figure 5b is a typical example of such a computer-generated magnetic flux density contour map computed for the

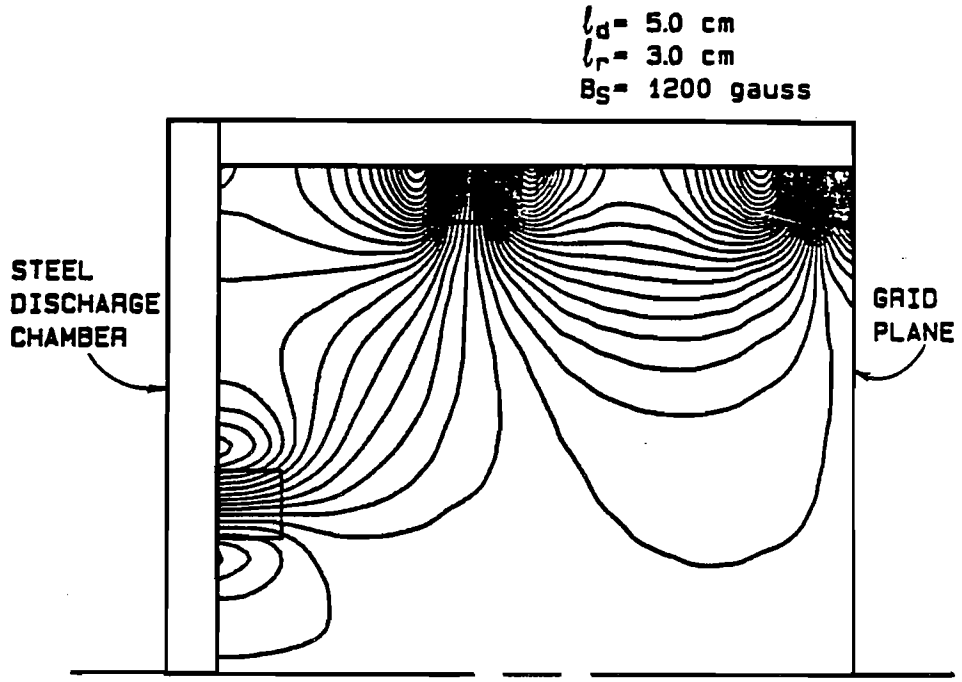

Fig. 5a Typical Pseudo Iron Filings Map (Computer Generated)

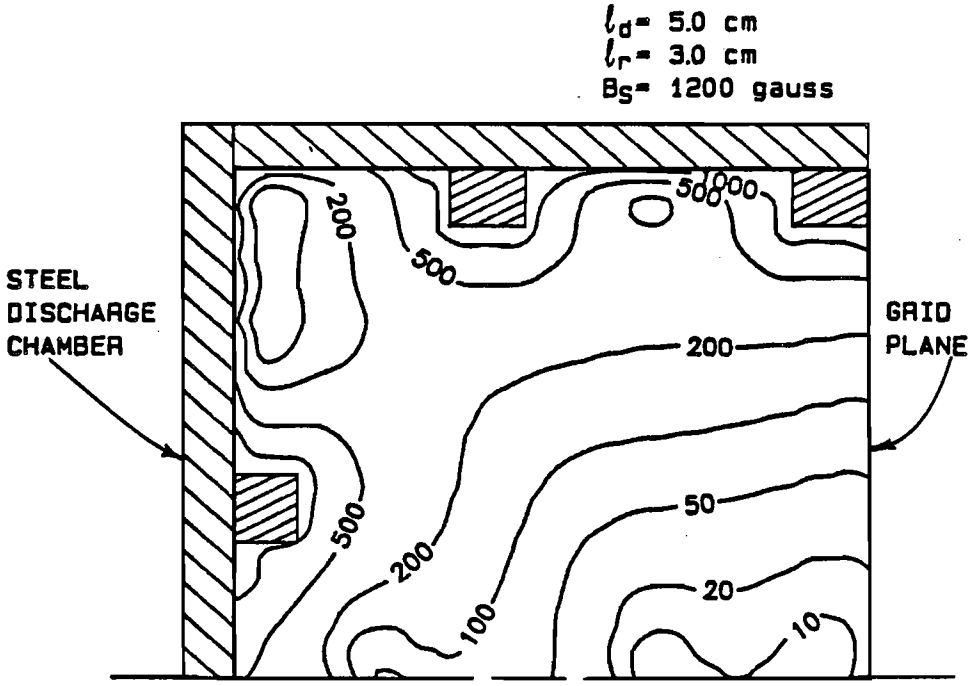

Fig. 5b Typical Magnetic Flux Density Contour Map
(Computer Generated)

same discharge chamber and magnet configuration that produced the filings map shown in Fig. 5a. It should be noted that flux density scaling between equal flux density contours is logarithmic with distance. The maps shown in Fig. 5a and 5b have been verified experimentally in several permanent magnet discharge chambers and they are considered to be reliable. Therefore, computer generated maps like those shown in Fig. 5a and 5b will be used throughout this study to describe discharge chamber magnetic field environments and to explain why magnetic field variations (eg. changes in magnet position and strength induce changes in performance.

IV. EXPERIMENTAL RESULTS

Experimentally measured discharge chamber performance can be described using plasma ion energy cost (ϵ_p) vs. discharge chamber neutral density parameter ($\dot{m}[1 - \eta_u]$) plots like the example shown in Fig. 6. These particular data were recorded with the discharge chamber having the configuration described by the parameters listed in the legend (and defined in Fig. 3) when the flux density (B_S) at the surface of each magnet was 1200 gauss. The theory developed by Brophy [5] suggests the experimental data of Fig. 6 should be fit by Eq. (2) when the parameters ϵ_p^* (the baseline plasma ion energy cost) and C_0 (the primary electron utilization factor) are determined properly. In the case of the data shown in Fig. 6 non-linear, least-squares curve fitting of the experimentally determined data points shown yielded the curve and values of these parameters given on the figure. The data and the curve show sufficiently good correlation to suggest that the values for ϵ_p^* and C_0 can be used in Eq. (2) to define discharge chamber performance with reasonable accuracy. The correlation between the curve computed using the performance parameters and the measured data shown in Fig. 6 shows the extent to which values for these two parameters could typically be used to describe experimentally measured performance data in this study.

The other parameter needed to describe discharge chamber performance is the extracted ion fraction (f_B) which is computed from the same experimental data used to generate data like those shown in

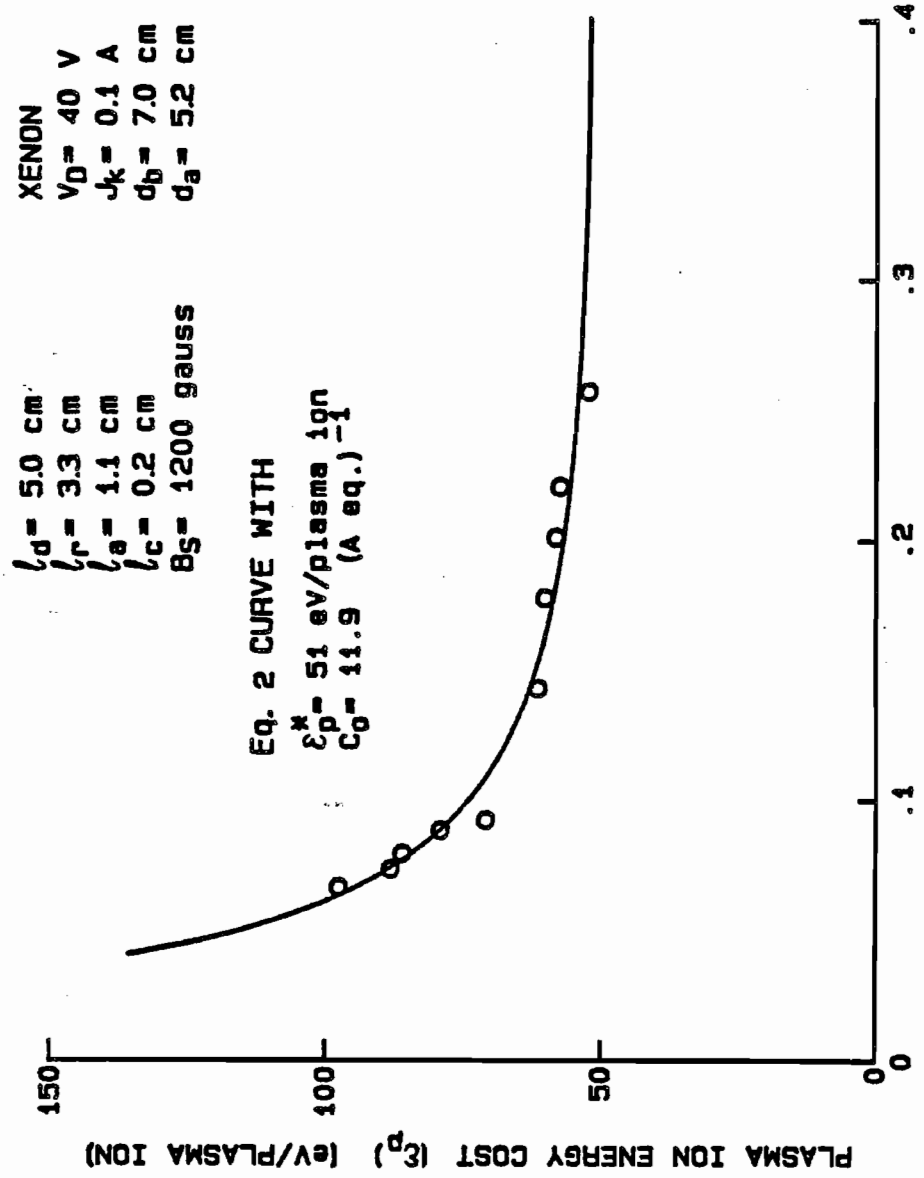

Fig. 6 Typical Discharge Chamber Performance Data

Fig. 6. The value of this parameter is, however, independent of the neutral propellant density in the discharge chamber (i.e. independent of neutral density parameter as demonstrated by Brophy [5]) so a single value of this parameter can be cited directly from measured data. For the particular discharge chamber defined by the parameters in the legend of Fig. 6, the extracted ion fraction was 0.31.

The advantage of describing discharge chamber performance in terms of the parameters C_0, ϵ_P^* and f_B is that each of the parameters relates to specific aspects of performance so comparison of measured values of these parameters to standard ones enables one to identify the mechanisms responsible for changes in discharge chamber performance. For example one can determine if changing the location of the anode causes a detrimental change in performance and the extent to which this change causes increased losses of primary electrons to the anode (a decrease in C_0), increased losses of ions to hollow cathode or anode surfaces, or an increase in the average energy of Maxwellian electrons being collected by the anode (an increase in ϵ_P^*), or increased losses of ions to some other discharge chamber surface (a decrease in f_B).

It should be noted that a knowledge of the values of ϵ_P^*, C_0 and f_B is sufficient to enable one to compute the associated beam ion energy costs of a chamber as a function of propellant utilization efficiency if an operating condition is specified (through application of Eq. 1). Therefore, all experimental results presented in this study will be presented as a function of these three performance parameters.

The Comparative Behavior of Refractory Filament and Hollow Cathodes on Performance

When a filament cathode electron source is used in a discharge chamber one can control the shape and location of the region from which primary electrons are supplied, but with a conventional hollow cathode one has generally been limited to electron emission from a point on the discharge chamber centerline. A question that arises is whether a filament cathode emitting electrons from a point on the discharge chamber centerline would give the same performance as a hollow cathode emitting from the same point. In order to address this question an experiment was conducted in which the discharge chamber shown in Fig. 3 was operated using a hollow cathode and its performance was then compared to that achieved using a small diameter (2 mm) coiled filament positioned at the axial location previously occupied by the hollow cathode orifice. The discharge chamber remained unchanged from that shown in Fig. 3 except for the cathode substitution.

Figure 7 shows the comparative plasma ion energy cost vs. neutral density parameter and extracted ion fraction data measured with the cathodes positioned downstream of the cusp at $\ell_c = 0.2$ cm and the rest of the discharge chamber parameters as listed in the legend. The data show no substantial differences in either the extracted ion fraction or the primary electron utilization factor, however, the baseline plasma ion energy cost for the hollow cathode is approximately twice that of the filament cathode. These large differences in baseline plasma ion energy cost can be accounted for by recognizing that the primary electrons acquire an energy approximately equal to the difference between the potential of the anode and the electron source potential. In the case of the filament cathode this energy is equal to the

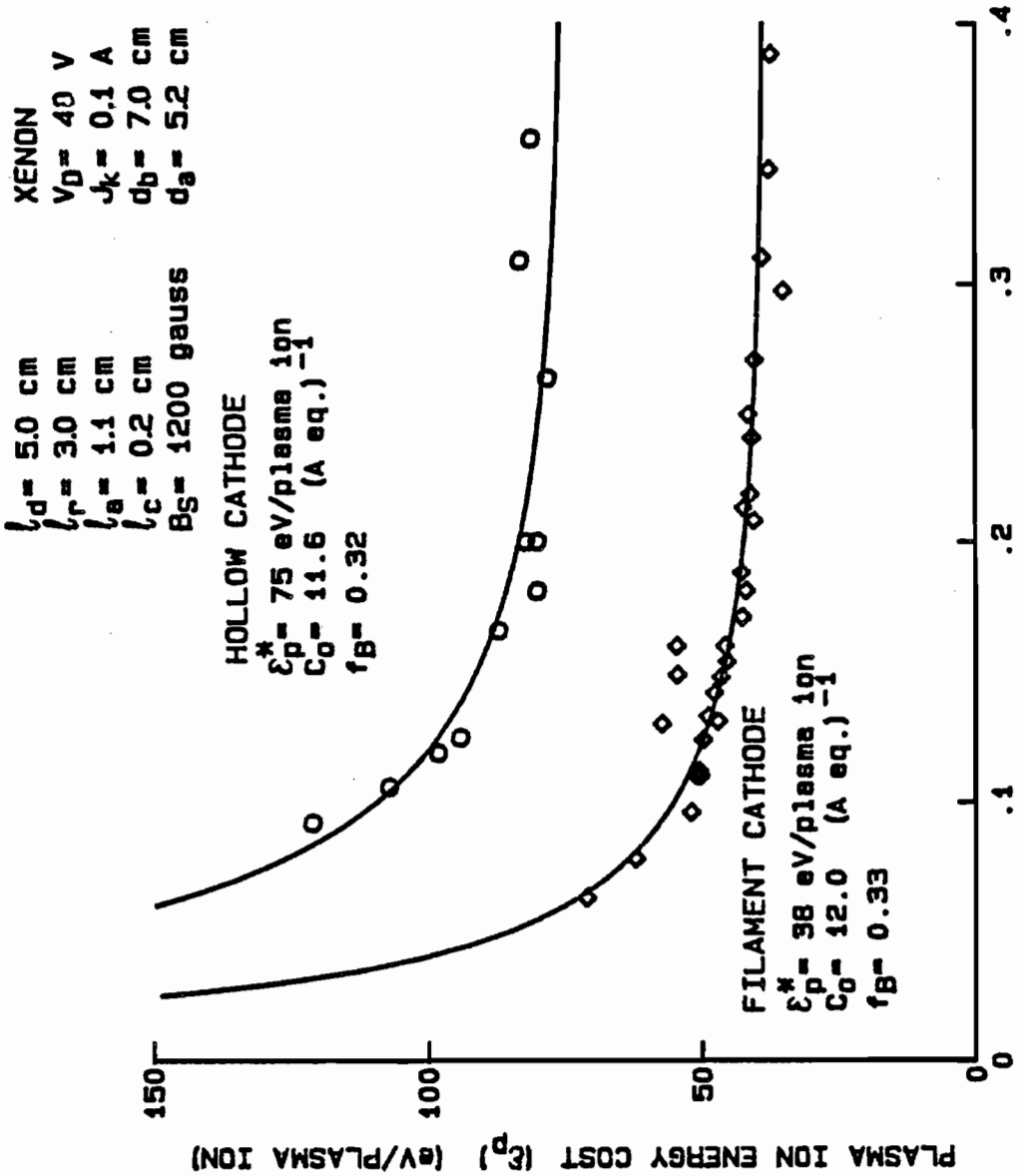

Fig. 7 Hollow Cathode/Filament Cathode Performance Comparison

cathode-to-anode potential difference (i.e. the discharge voltage) and in the case of the hollow cathode it is the difference between the plasma potential immediately adjacent to the cathode and anode potential. Because the plasma potential adjacent to the hollow cathode orifice is always higher than cathode potential and because the discharge voltage is the same for both cases, each electron coming from the hollow cathode supplies less energy to the discharge than does one coming from the filament cathode. The equation used to compute plasma ion energy costs (ϵ_p values from Eq. (4)), however, ascribes an energy equal to the full discharge voltage to each electron in both cases and the ion energy cost associated with the ion production process is computed incorrectly in the case of the hollow cathode system.

In order to compute the primary electron energy that will yield the correct value of ϵ_p, the primary electron acceleration process is broken into two series processes, namely the one associated with acceleration of electrons from the cathode insert to the adjacent plasma and a second associated with acceleration from this plasma to the discharge plasma (which is assume to be near anode potential). When Eq. (4) is derived considering primary electron acceleration from a plasma potential (V_k) adjacent to the hollow cathode, it becomes

$$\epsilon_p = \frac{(V_D - V_k)(J_D - J_P)}{J_P} . \qquad (8)$$

The potential difference ($V_D - V_k$) which appears in this equation represents the kinetic energy the primary electrons have as they enter the discharge chamber. If a filament cathode is used, electrons are

accelerated into the discharge from its surface, V_k is zero and Eq. (4) results.

For the present tests the keeper voltage (V_k) was used as the best available measure of the plasma potential adjacent to the hollow cathode. It was also recognized, however, that the point at which the electrons begin accelerating into the chamber is not known and that primary electron collisional losses at the cathode increase with hollow cathode flowrate. In view of this the value of keeper potential (V_k) measured at a low cathode flowrate where it should be closest to the potential of the internal cathode plasma was selected as most representative of the hollow cathode electron source potential.

During the conduct of the tests using the hollow cathode, the keeper voltage generally varied from 12 V at low values of discharge chamber neutral density parameter (high cathode flowrates) to 20 V at high values of discharge chamber neutral density parameter (low cathode flowrates). If the electron source potential was assumed to be equal to that of the keeper at low cathode flowrates (~20 V) and Eq. (8) was used to calculate plasma ion energy costs associated with the circular symbol data of Fig. 7, the hollow cathode data (circular symbols) shown in Fig. 8 were computed. These data show good agreement between all parameters (ϵ_p^*, C_0 and f_B) for the filament and hollow cathode cases and this suggests that discharge chamber performance obtained using a hollow cathode is comparable to that obtained with a filament cathode when hollow cathode operating power is properly removed from the baseline plasma ion energy cost.

It is noted that substitution of the keeper voltage measured at each discharge current condition into Eq. (8) (rather than using the constant 20 V value that produced the results of Fig. 8) yielded poorer

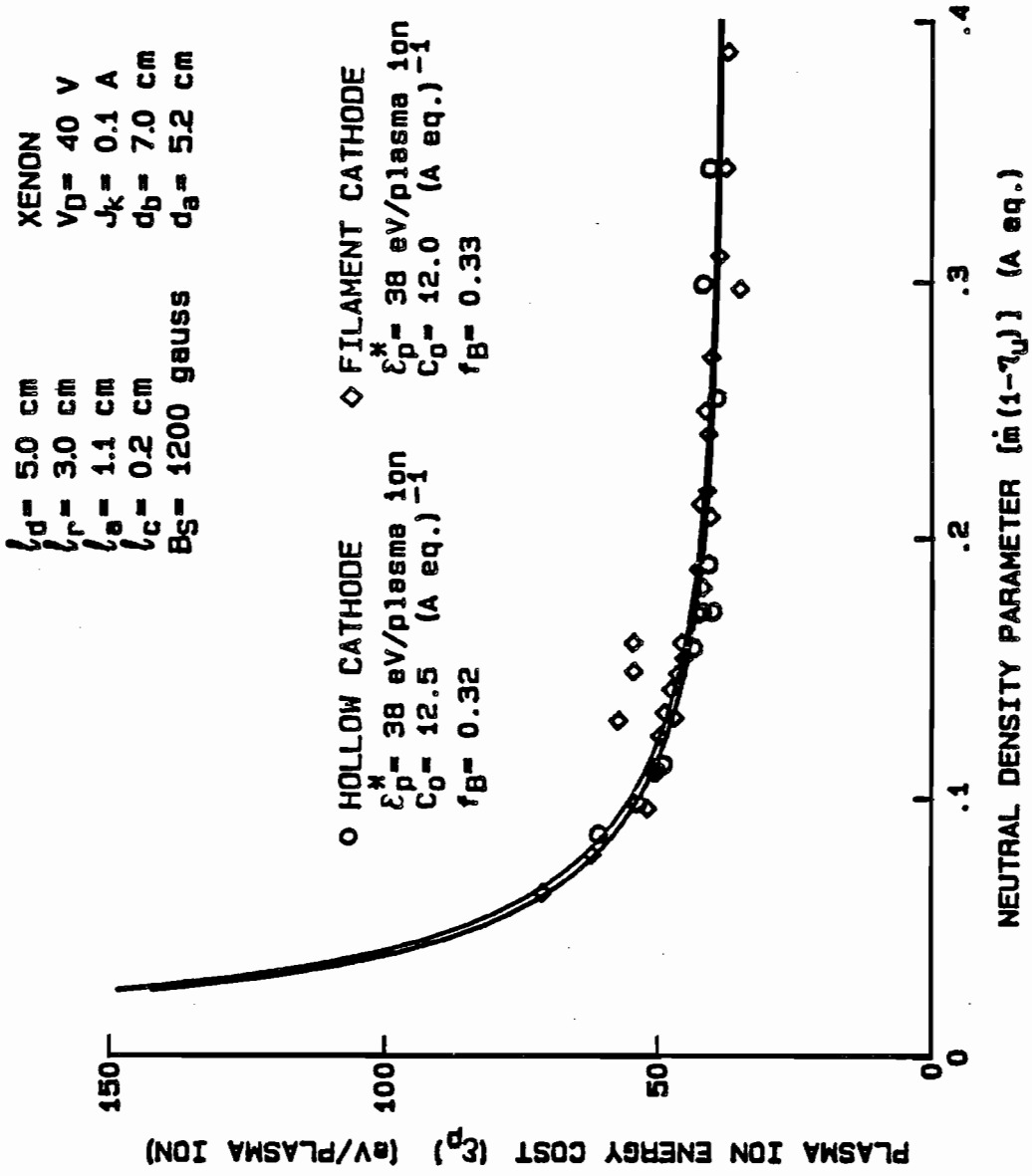

Fig. 8 Hollow Cathode/Filament Cathode Performance Comparison (with Keeper Potential Correction)

agreement between the least squares curve fit values of both ϵ_P^* and C_0 for the two cathodes. While it may be that electrons are being supplied from this higher potential as keeper voltage changes, more research into the subject of hollow cathode vs. filament cathode effects on discharge chamber performance to enhance understanding of the phenomena that are occurring is considered desirable.

The Effects of Varying the Region of Electron Injection (Cathode)

Because ion thrusters cathodes have generally been located at the upstream end of the discharge chamber on the centerline this cathode location was selected as the starting point for a study of the effects of cathode position on discharge chamber performance. A filament cathode was used in these initial studies because its size and location can be varied easily. After completion of the upstream filament cathode study in which both the diameter and axial position of the cathode were varied, the effects of changing axial position only were investigated using a hollow cathode.

Cathode Diameter and Axial Location (Upstream of Ring Cusp)

During these tests data similar to those shown in Fig. 6 were recorded at each filament cathode diameter (d_c in Fig. 2) and axial position (ℓ_c in Fig. 2) to determine how they influenced the discharge chamber performance parameters ϵ_P^* and C_0. Figure 9 shows the effects induced by varying the diameter of the filament cathode from 0.2 cm to 3.2 cm on ϵ_P^* and C_0. The data presented in Fig. 9 were recorded with the discharge chamber configured as described by the dimensions shown in the legend and defined in Fig. 2. These data show that reducing the diameter of the filament from 3.2 cm to 0.2 cm has no significant

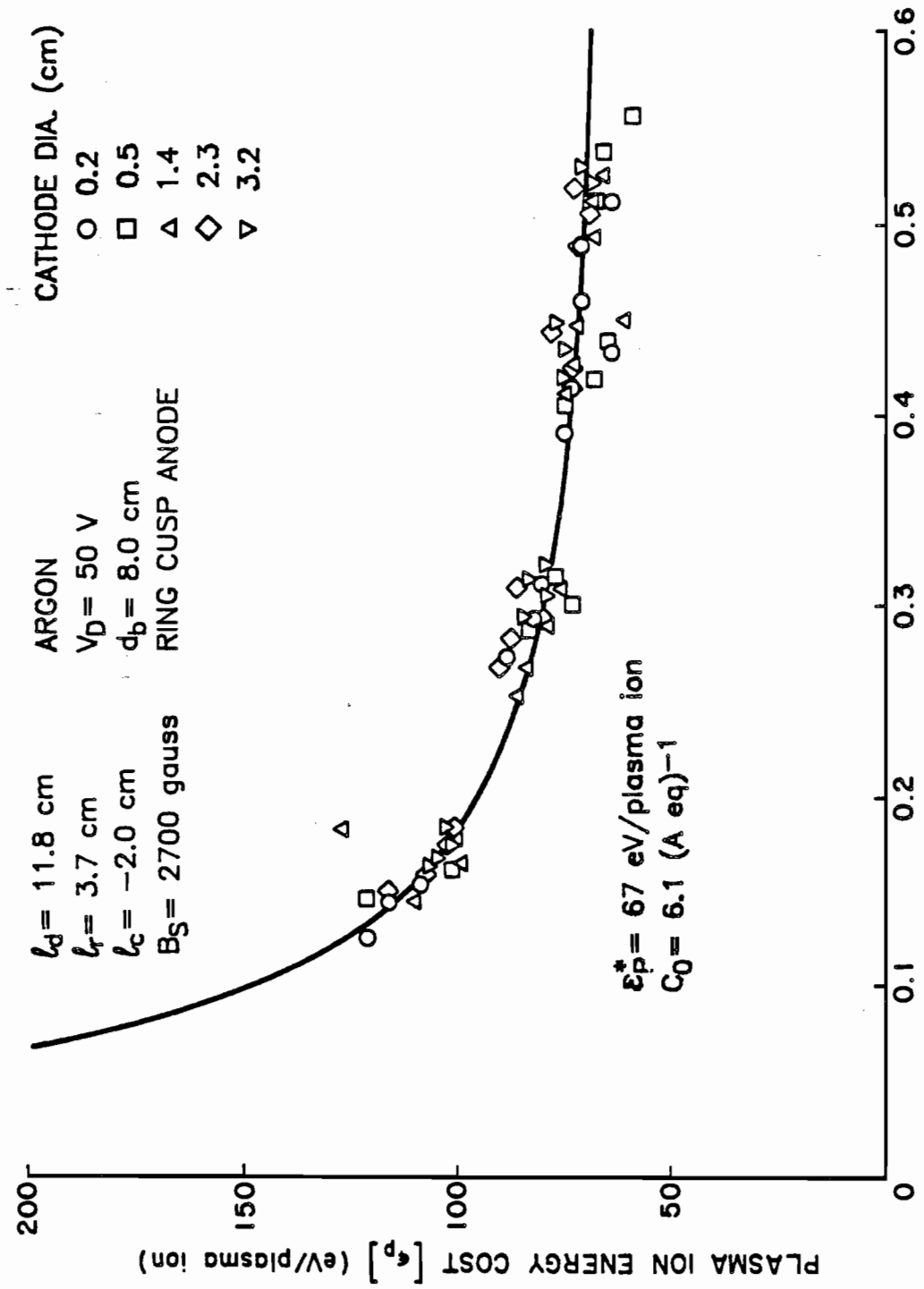

Fig. 9 Effect of Upstream Filament Cathode Diameter on Plasma Ion Energy Cost Curve

effect on ϵ_P^* or C_0. This result is significant because changing the cathode filament diameter changes the magnetic field line onto which the primary electrons are released upstream of the ring magnet into the discharge chamber. This in turn indicates the distance an average primary electron travels (ℓ^*) if it has no collisions before it reaches an anode located on the ring cusp is the same regardless of the field line onto which it is emitted (C_0 does not change) when the cathode is upstream of the cusp. Because ϵ_P^* does not change either, it is also logical to conclude that the average energy (or temperature) of the Maxwellian electrons being collected by the anode does not change significantly as cathode diameter is changed. It should be pointed out that these observations may be different if the tests could be conducted using a loop rather than a ring cusp anode or if the cathode were located downstream of the cusp.

When the cathode axial position was changed from $\ell_c = -2.0$ cm (data of Fig. 9) to $\ell_c = -0.7$ cm upstream of the cusp and data similar to those shown in Fig. 9 were recorded, they fell along a slightly different line as the two curves shown in Fig. 10 suggest. These curves show that changing cathode axial position induces no significant change in ϵ_P^* but moving the cathode downstream toward the plane of the ring cusp does cause C_0 to decrease slightly thereby suggesting poorer primary electron containment. Moving the primary electron source closer to the anode might be expected to facilitate increased primary electron losses to the anode but the fact that increasing cathode diameter, which also moves the electron source closer to the anode, did not produce a similar effect, makes these two results somewhat inconsistent.

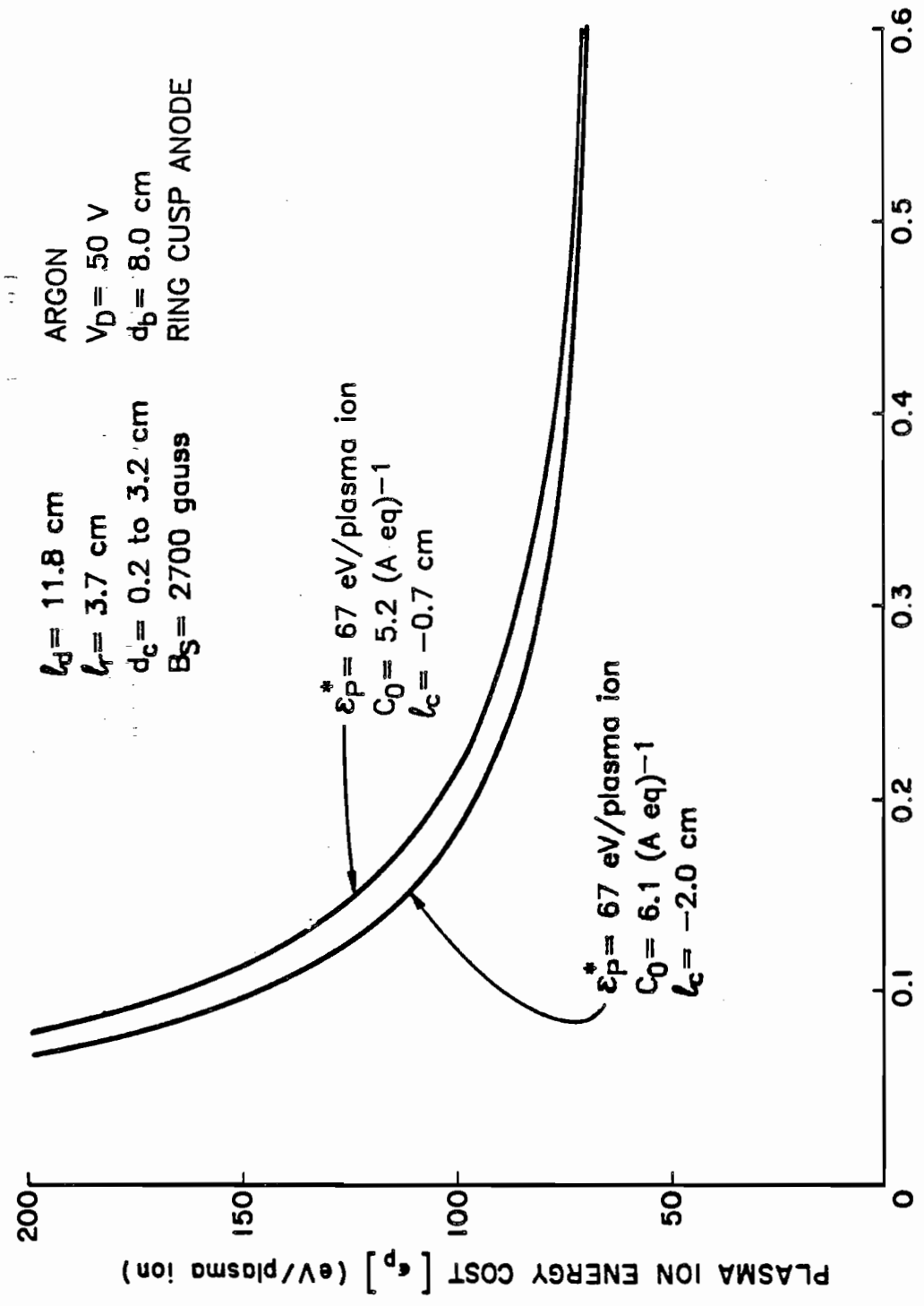

Fig. 10 Effect of Upstream Filament Cathode Axial Position on Plasma Ion Energy Cost Curve

The final parameter needed to describe the effects of cathode diameter and position on discharge chamber performance is the extracted ion fraction (f_B). The changes induced in f_B by variations in cathode diameter and position are presented in Fig. 11. These data, which were collected at the same time as those shown in Figs. 9 and 10, show a reduction of about a factor of three in the extracted ion fraction as the diameter of the filament cathode is increased from 0.2 cm to 3.2 cm and a more modest increase in f_B as the cathode is moved downstream toward the axial reference location (ℓ_c = 0 cm). It is interesting to note that if the filament cathode diameter is small (d_c = 0.2 cm) changing its axial position induces no significant changes in any of the performance parameters (hence no change in performance) for this case where the electrons are being collected on a ring anode and the cathode is upstream of the cusp.

Insight into the reason for the decrease in the extracted ion fraction as a function of filament diameter can be gained by examining the magnetic flux density contour map for this particular discharge chamber which is shown in Fig. 12. In this particular map a region of low magnetic flux density exists upstream of the ring cusp near the discharge chamber walls. When the zone of electron emission (and therefore increased ionization) is moved closer to the discharge chamber walls by increasing the filament cathode diameter the ion losses across this low flux density region (due to Bohm diffusion) increase and cause f_B to decrease. Also, it should be noted that the flux density near the discharge chamber walls is smaller 2.0 cm upstream of the ring cusp than it is 0.7 cm upstream of it. This decrease causes the decrease in extracted ion fraction as a function of cathode position (ℓ_c).

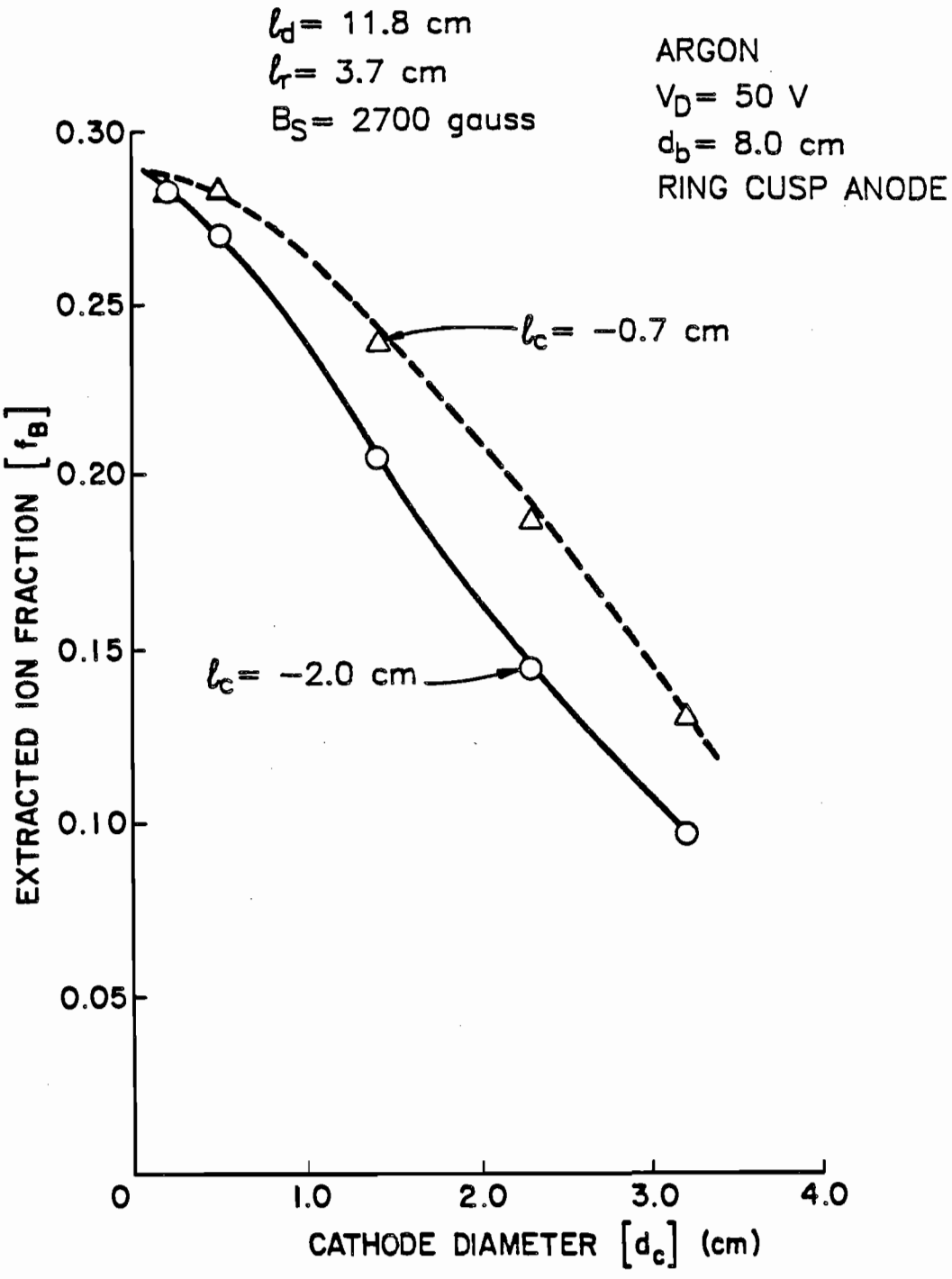

Fig. 11 Effects of Upstream Filament Cathode Diameter and Position on Extracted Ion Fraction

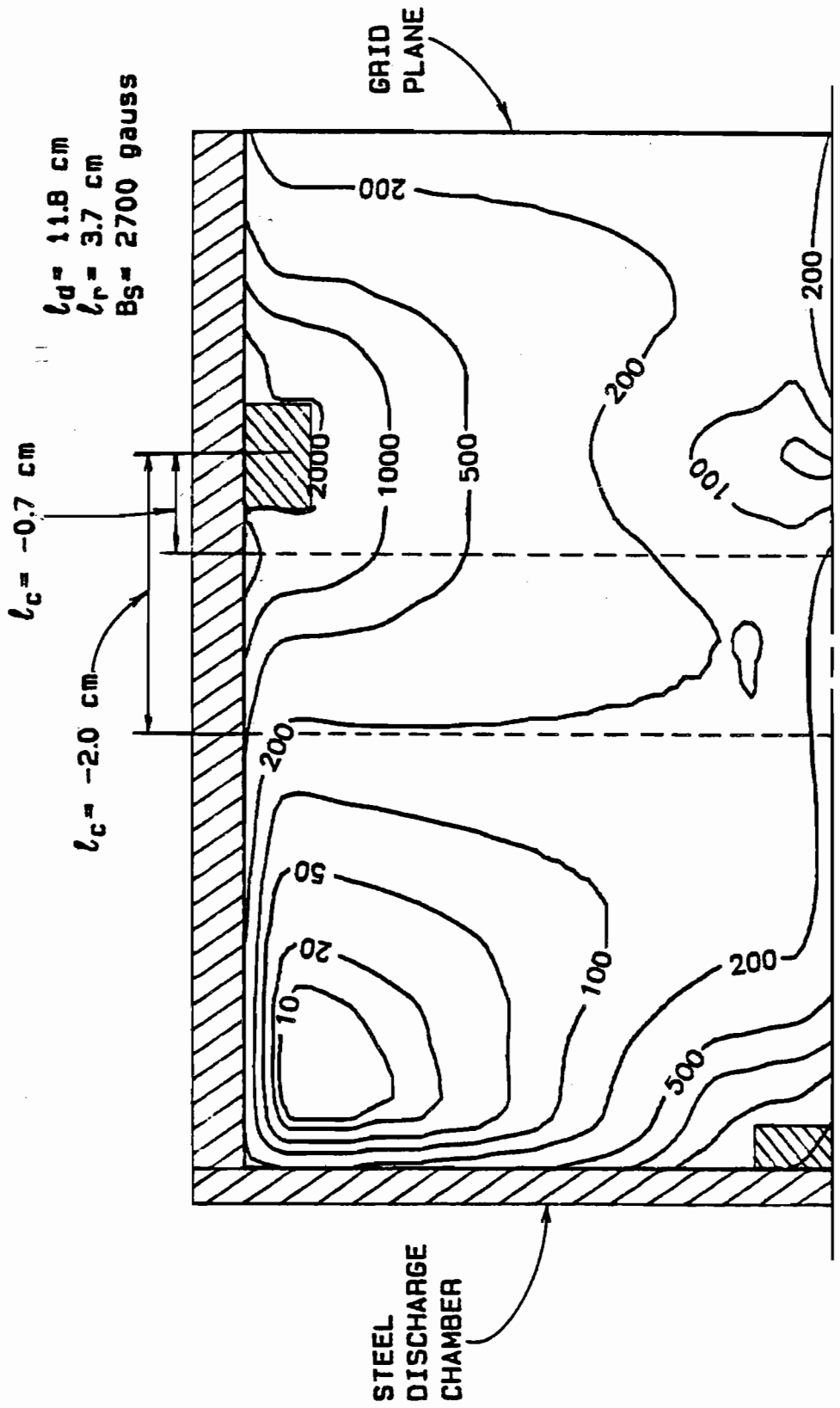

Fig. 12 Magnetic Flux Density Contour Map (l_d= 11.8 cm)

Finally, it is noted that Hiatt [1] found that increasing filament cathode diameter yielded improved discharge chamber performance. This is entirely consistent with the trends shown here because his tests were performed with the cathode filament located downstream of the cusp next to the grids, where increasing cathode diameter facilitates increased production of ions near the outer radii of the ion extraction system. These ions can be readily extracted because they are produced near the grids which increases the extracted ion fraction and, hence, the performance.

Hollow Cathode Axial Position

The effect of hollow cathode axial position along the discharge chamber centerline was examined using xenon propellant in the apparatus shown in in Fig. 3. Because this propellant is different than that used for the filament cathode tests, trends associated with cathode movement rather than direct comparisons of the values of C_0 and ϵ_P^* between the tests will be made. In the hollow cathode tests a loop anode was used and its axial position downstream of the cusp, its diameter and the magnetic field configuration of the chamber were held fixed. It is interesting to note that in this case, contrary to cases where the discharge chamber of Fig. 2 was used, the discharge could be sustained using the loop anode alone. It is speculated that the three anode support posts protruding through the cusp region (Fig. 3 apparatus), which are not present in the Fig. 2 apparatus, acted as a keeper that helped to sustain the main discharge to the anode [6].

The conduct of these tests involved the generation of discharge chamber performance plots like those in Fig. 6 at each cathode position and the subsequent determination of discharge chamber performance

parameters (ϵ_p^*, C_0 and f_B) using Eqs. (2) and (6). Figure 13 shows the variation in these parameters as a function of hollow cathode position over the range $-0.6 \leq \ell_c \leq 0.5$ cm (i.e 0.6 cm upstream to 0.5 cm downstream of reference location). These data suggest the primary electron utilization factor is not affected by cathode position and this is consistent with the data obtained in the upstream filament cathode test. On the other hand both the baseline plasma ion energy cost and the extracted ion fraction increase as the hollow cathode is moved upstream of the reference (central ring cusp) location--neither changed when the small diameter filament was moved. One of these effects is beneficial (increased extracted ion fraction) and the other is detrimental (increased baseline plasma ion energy cost). The fact that these curves show similar behavior suggests both parameters are being affected by a common phenomenon. The behavior shown in Fig. 13 could be explained qualitatively if upstream movement of the hollow cathode caused a fraction of the ions being lost to the chamber walls to be lost instead to the hollow cathode itself. This effect would cause both parameters to increase with upstream cathode movement because ions lost to the cathode are not measured and this therefore causes a decrease in the measured ion production current (J_p) which appears in the denominator of the expressions from which these parameters (Eqs. (4) and (5)) are computed.

A development presented in Appendix A can be used as a tool to understand that proportional changes in both ϵ_p^* and f_B like those shown in Fig. 13 can be explained if substantial ion losses are occurring to cathode and/or anode surfaces. This analysis indicates the baseline

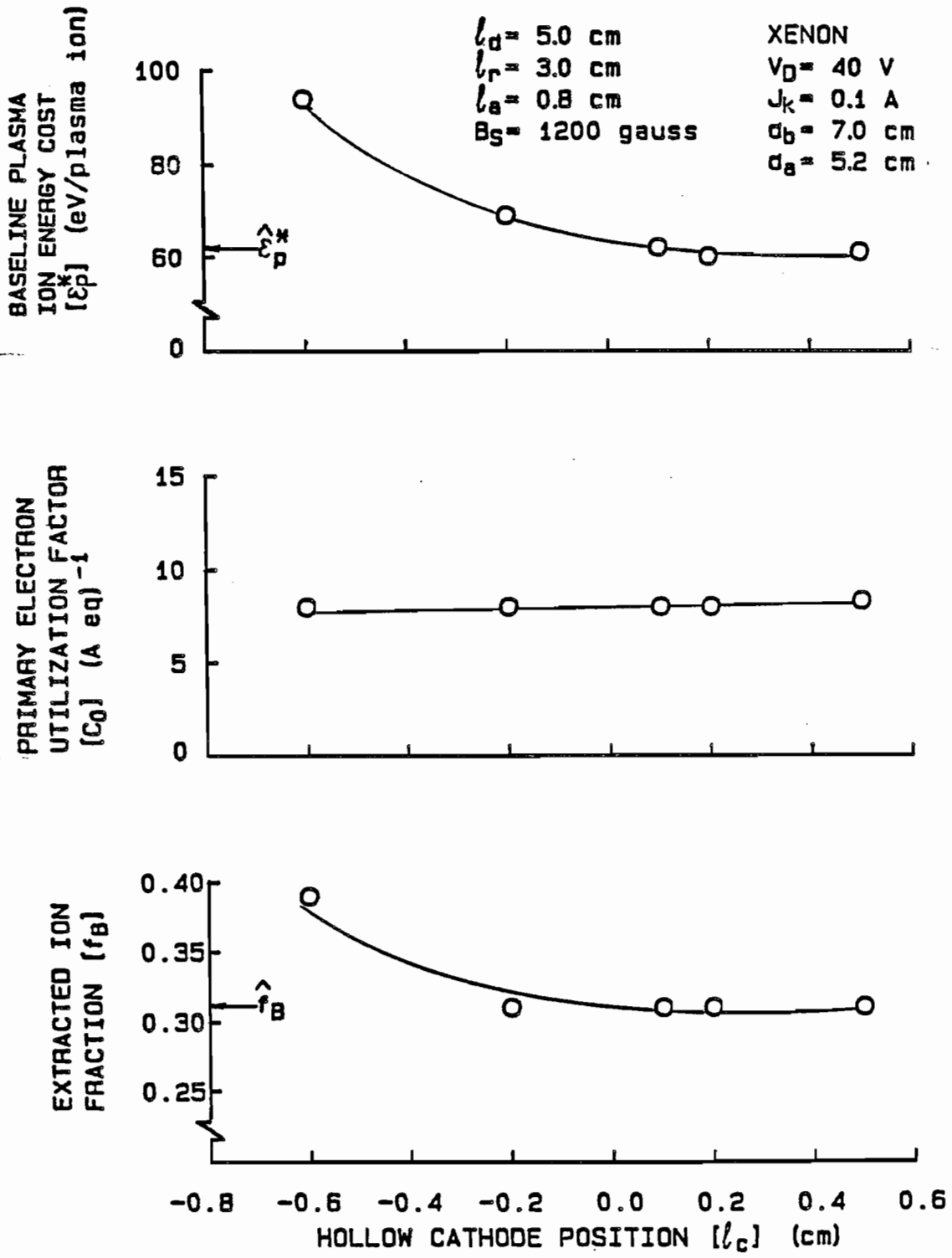

Fig. 13 Effect of Centerline Hollow Cathode Axial Position on Discharge Chamber Performance Parameters

plasma ion energy cost and the extracted ion fraction should satisfy the equation

$$f_B = \frac{\hat{f}_B}{\hat{\epsilon}_P^*} \epsilon_P^* \qquad (9)$$

where $\hat{f}_B$ and $\hat{\epsilon}_P^*$ (identified in Fig. 13) are the values of these parameters which are associated with performance measurements made with the cathode positioned in the downstream region where the ion loss rate to the hollow cathode or anode is negligible. This equation fits the data of Fig. 13 well, and it is believed that the unmeasured ions produced in the high density neutral plume from the hollow cathode are lost back to it when the cathode is positioned too far upstream. Such an effect would not be observed with a filament cathode because there is no high neutral atom density plume located at this cathode. Finally, it is noted that if the cost of operating the hollow cathode is accounted for in computation of the value of ϵ_P^* in the manner described previously (Comparative Behavior of Refractory Filament and Hollow Cathodes on Performance), Eq. (9) and the data of Fig. 13 fall into even better quantitative agreement.

All of these results taken together suggest that the increase in extracted ion fraction induced by upstream cathode movement is artificial and is compensated by a corresponding increase in baseline plasma ion energy cost to the point where no substantial net effect on beam ion energy cost is realized (see Eq. (1)). This result is qualitatively similar to results obtained in the upstream filament cathode tests.

The reason why ion losses to the hollow cathode increase as it is moved upstream can be understood by considering the centerline magnetic flux density profile shown in Fig. 14 which was measured along the chamber centerline using a gaussmeter. This profile shows upstream cathode movement places it in a progressively higher magnetic flux density environment. This would be expected to confine electrons (and therefore ions) progressively closer to the cathode and would promote ion losses to cathode surfaces at the expense of ion losses to the chamber walls.

It is noted that the data of Fig. 13 are limited to upstream cathode positions greater than -0.6 cm and Fig. 14 shows this is a region of negative flux density gradient. Movement of the hollow cathode upstream of the point of maximum flux density (~ -0.8 cm), however, caused the performance of the ion source to degrade rapidly because of what appeared to be a dramatic increase in the baseline plasma ion energy cost that overshadowed corresponding modest changes in extracted ion fraction [6]. Thus test results obtained by moving the hollow cathode axially suggest overall discharge chamber performance as reflected in beam ion energy costs, which vary to first order as ϵ_p^*/f_B (see Eq. (1)), are unaffected by cathode position as long as it is downstream of the extreme, centerline flux density point. As the cathode is moved into regions of higher flux density, however, a greater fraction of the ions produced near the hollow cathode appear to be lost directly back to it rather than to the chamber walls.

Cathode Diameter (Downstream of Ring Cusp)

The conventional position from which to emit electrons has been on the discharge chamber centerline because this is a convenient location

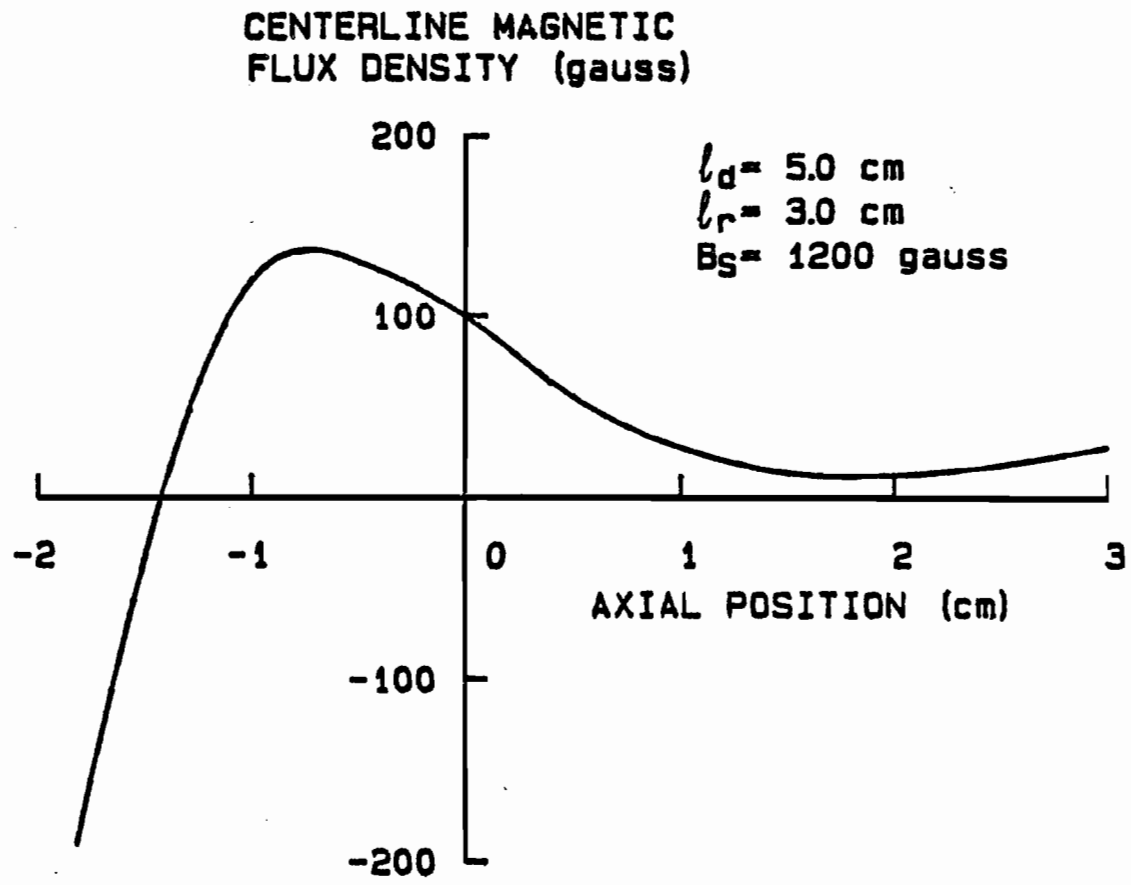

Fig. 14 Centerline Magnetic Flux Density Profile

that produces a symmetrical spatial distribution of primary electrons into the discharge chamber. If the region into which the electrons are supplied is relatively magnetic field free over a large region then these electrons can diffuse throughout the region producing ions. Because high flux density magnets were used in a rather small discharge chamber in these tests the magnetic field penetrated deep into the center of the discharge chamber thereby reducing the extent of the field-free region. A test was conducted to see if moving a cathode off of the discharge chamber centerline and thereby increasing the volume in which ionization could take place would enhance discharge chamber performance. The tests were performed using a refractory filament cathode in the test apparatus shown in Fig. 3. A refractory filament cathode was selected for these tests because it allowed precise control of primary electron injection into the chamber from an azimuthally uniform zone. Because it was shown in previous tests that a discharge chamber equipped with either a filament cathode or a hollow cathode produce similar discharge chamber performance when the cost of operating the hollow cathode is accounted for, it is suggested that a hollow cathode having an azimuthally oriented slit orifice at the same radius as that of the filament cathode used in these tests would exhibit similar performance.

The results of this test which are presented in terms of the three performance parameters as a function of filament cathode diameter (d_c) are shown in Fig. 15. The data in this figure were recorded with the discharge chamber configured as shown in the legend. When the filament cathode diameter is increased from 0.2 cm to 2.8 cm the zone of primary electron injection into the discharge chamber plasma is moved closer to

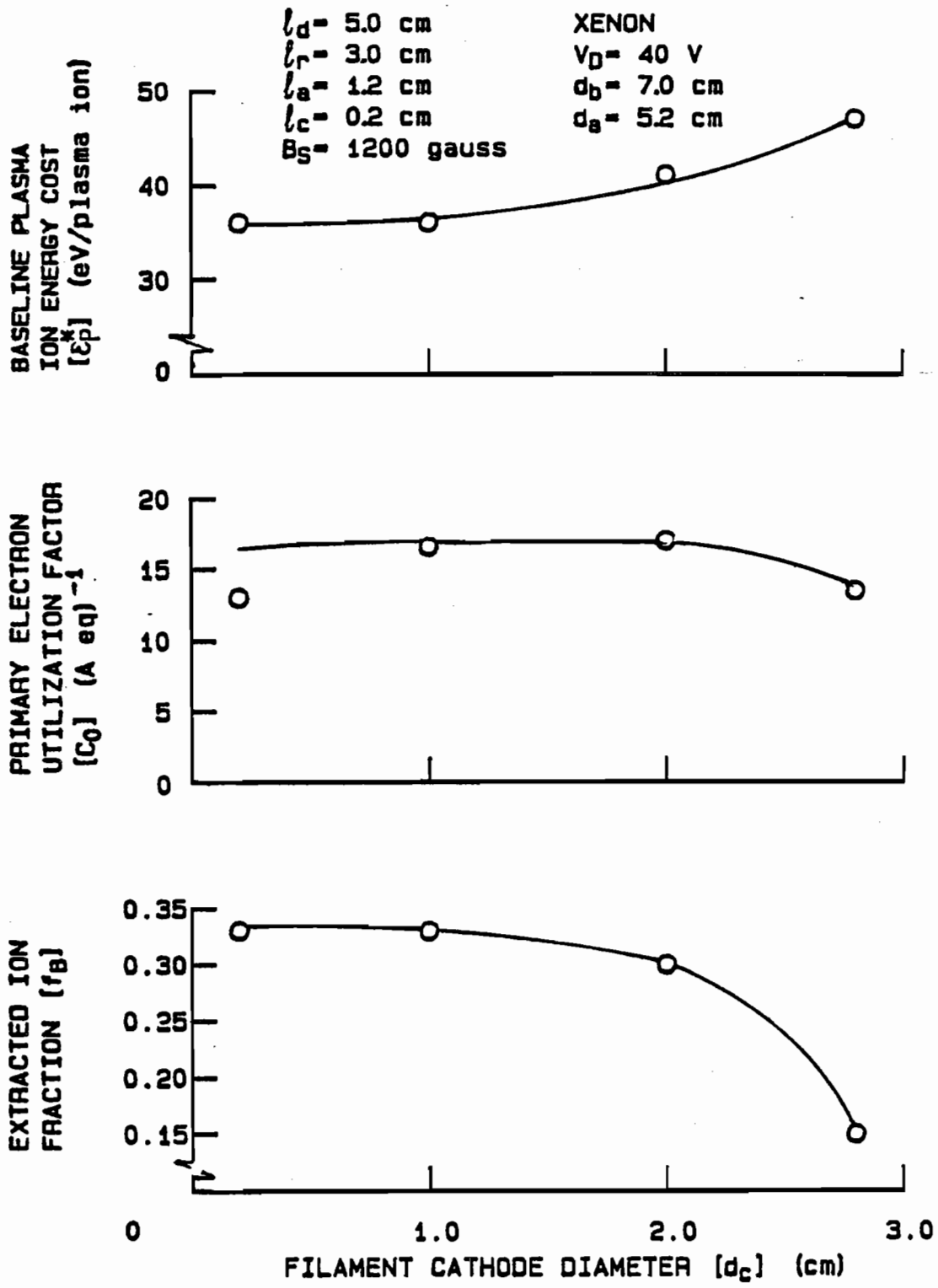

Fig. 15 Effects of Downstream Filament Cathode Diameter on Discharge Chamber Performance Parameters

the anode (and closer to the chamber walls) and this induces increased ion production near this zone. As the data suggest, this causes 1) the average energy of Maxwellian electrons being collected at the anode to increase (an increase in ϵ_p^*), 2) the primary electron containment length to decrease (C_0 decreases) and 3) the fraction of ions being lost to the discharge chamber surfaces to increase (f_B decreases).

Finally, it is noted that Hiatt [1] observed an increase in the extracted ion fraction as cathode diameter was increased. this appears to contradict the data of Fig. 15, however, in the present case the anode position remained constant (ℓ_a = 1.2 cm) while Hiatt adjusted the anode position at each cathode diameter to realize optimum performance (see Anode Position). It is, also, noted that there is substantial uncertainty associated with the value of C_0 shown in Fig. 15 for the smallest filament cathode diameter because this data point is based on a small amount of experimental data.

Anode Position

Hiatt [1] showed that discharge chamber performance continues to improve as the anode is moved downstream of the axial reference location to the position where the discharge goes out. It was suggested that the downstream movement of the anode improved performance because it reduced the loss rates of higher energy Maxwellian and primary electrons to the anode. This trend continued until the orthogonal line integral of the magnetic field between the virtual cathode and anode surfaces became so great that the discharge could not be sustained at the prevailing discharge voltage. Similar results were also observed in the present study where a hollow cathode was used in place of the filament cathode. However, in the case of the

hollow cathode experiments, an actual extinction of the discharge was generally not observed. Rather the discharge current would decrease until it became too small to produce significant numbers of ions as the anode was moved downstream and the discharge voltage and propellant flowrate were held constant. The higher the discharge voltage and propellant flowrate the further downstream the anode could be moved before this situation developed.

Typical experimental results obtained during a test designed to investigate the effects of axial anode movement on discharge chamber performance are presented in Fig. 16 and they are qualitatively similar to data obtained by Hiatt [1] in a filament cathode-equipped discharge chamber. The data were recorded using a chamber with the dimensions shown in the legend when the magnetic surface flux density (B_s) was 1200 gauss. The data points shown at ℓ_a= 0.96 cm were recorded with the anode just upstream of the operating point where the maximum discharge current that could be drawn dropped precipitously at nominal discharge voltage and total flow conditions (40 V and ~150 mA eq (Xe)). Because the propellant, discharge voltage and electron source potential (keeper voltage) were constant for these tests it is argued that the decrease in baseline plasma ion energy cost with downstream anode movement is caused by the decrease in the average energy of Maxwellian electrons being collected at the anode that has been observed previously [1,5]. This preferential collection of progressively lower energy electrons as the anode is moved downstream occurs because the momentum transfer collision cross section for electrons with atoms and ions increases as electron energy decreases. Hence as the anode is moved to magnetic field lines progressively further from those which intersect the cathode orifice (i.e. the anode is moved downstream

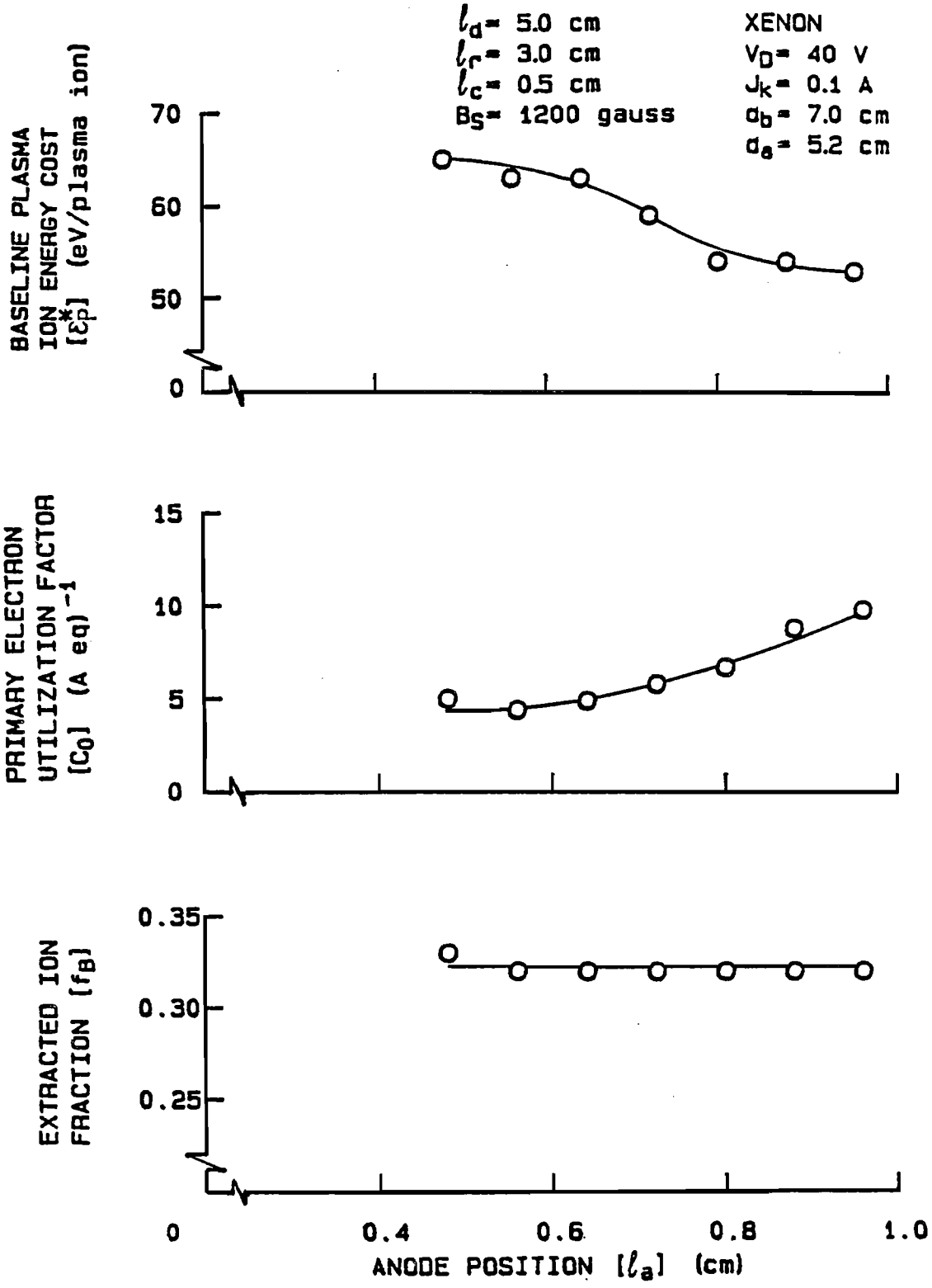

Fig. 16 Effect of Anode Position on Discharge Chamber Performance Parameters

electrons which have low energies (and therefore have many momentum transfer collisions) are most likely to migrate across magnetic field lines and reach the anode. Thus, downstream movement of the anode reduces the average energy of the Maxwellian electrons reaching the anode and this induces the observed decrease in ϵ_P^* as ℓ_a is increased.

The primary electron utilization factor (C_0) is observed to increase as the anode is moved downstream. Because the primary electrons have an energy that is high compared to that of the Maxwellian electrons, they have low collision probabilities and therefore cannot cross field lines easily. As the anode is positioned further downstream the number of field lines that must be crossed to reach the anode increases, therefore the primary electron loss rate decreases and the primary electron utilization factor increases to reflect this.

Finally Fig. 16 shows the extracted ion fraction remains constant as the anode is moved downstream. This indicates that the total ion production rate and the beam current are changing at the same rate. During typical experiments the beam current was observed to increase as the anode was moved downstream and the discharge voltage, current and total flowrate were held constant--this was accomplished by adjusting the flow distribution between the hollow cathode and the discharge chamber flowrates. It is obvious from looking at Fig. 16 that this increase in beam current occurred because downstream anode movement induces an increase in C_0, a decrease in ϵ_P^* and no change in f_B. Physically this occurs because the energy in both the primary and Maxwellian electron groups is being better utilized to make ions and the fraction of these ions that escape the discharge chamber into the beam is remaining constant as the anode is moved downstream.

Magnetic Field Investigation

The magnetic field configuration in a discharge chamber is important because it must contain the ions away from the chamber walls and direct them toward the screen grid where they can be extracted into the beam. Two criteria that should be met for a good magnetic field design are: 1) a sufficiently high magnetic flux density near the surface of the discharge chamber walls to ensure proper ion containment and 2) proper positioning of the ring magnet so that the entire surface of the screen grid is exposed to the discharge chamber plasma. These criteria were difficult to meet simultaneously with the small diameter discharge chamber used in these tests because the magnets used in this study were relatively large and produced fields that tended to penetrate deep into the chamber and reduce the low field strength volume in it. However, effects associated with these criteria were investigated by changing the flux density of the magnets and the axial location of the central ring magnet (i.e. varying ℓ_r shown in Fig. 3).

Magnetic Flux Density Variation

Tests to investigate the effects of magnetic flux density near the discharge chamber walls were conducted by varying the magnetic flux density measured at the surface of the steel strips and washer (Fig. 3). The steel was required in these tests to distribute the magnetic flux uniformly at each ring magnet surface. When the magnetic flux density was varied from 350 gauss to 2700 gauss the discharge chamber performance parameters varied in the manner shown in Fig. 17. These data suggest that increasing the magnetic flux density from 350 gauss induces 1) slightly reduced energy losses associated with Maxwellian electron collection at the anode (ϵ_P^* decreases with B_S), 2)

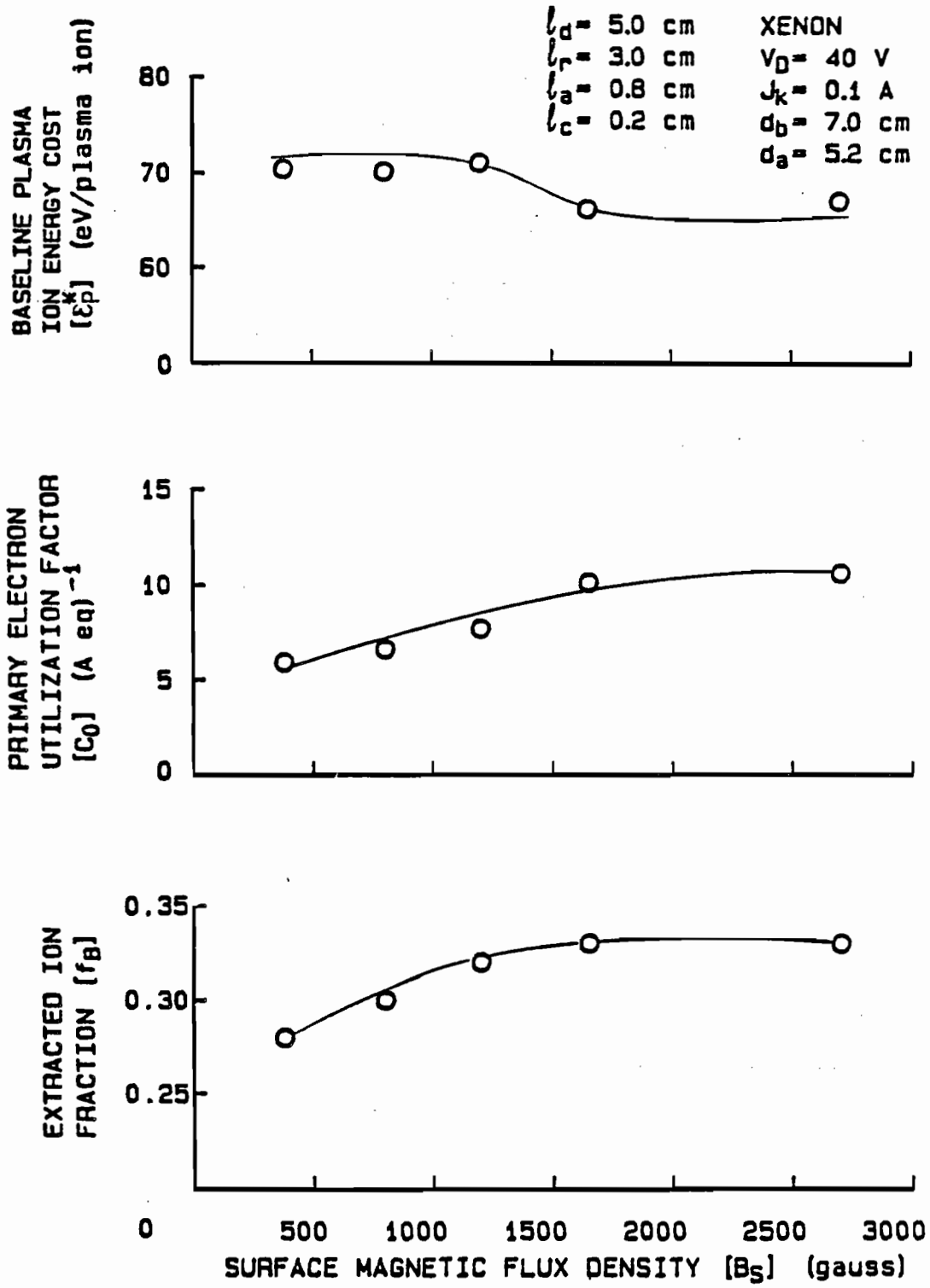

Fig. 17 Effect of Magnet Strength on Discharge Chamber Performance Parameters

improved primary electron containment (C_0 increases with B_S) and 3) improved ion containment (f_B increases with B_S). All of these trends improve performance and they are most significant over the magnetic flux density range from 350 to 1200 gauss. Beyond 1200 gauss the improvements in all of the parameters appear to be small.

The increase and subsequent leveling off of the extracted ion fraction shown in Fig. 17 is considered to be a consequence of the fact that two diffusion mechanisms (ambipolar-along magnetic field lines and Bohm diffusion-across them) determine net plasma motion in the discharge chamber. The discharge chamber plasma can diffuse readily (at the ambipolar diffusion rate) to cusps like those shown the iron filings map of Fig. 18. Electrons will generally be reflected from the magnets used in this study because the magnets are maintained near cathode potential, but significant numbers of ions can be lost to these magnet surfaces. This ion loss rate is believed to have a relatively weak dependence on magnet strength. Ions and electrons can also be lost by diffusing more slowly (at the Bohm diffusion rate) across field lines. In this case the highly mobile electrons will generally be lost to the anode once they reach the field line which intersects it, while the more massive ions will generally be lost to the discharge chamber walls or reflected back towards the core of the discharge as they attempt to move toward the walls and find a positive space charge induced by the absence of electrons. This loss of ions to the walls appears (based on the data of Fig. 17) to decrease as the magnetic flux density increases until at some surface magnetic field strength at the magnet rings (presumably near 1200 gauss in the case of the chamber configuration associated with the data of Fig. 17) the ion loss rate to

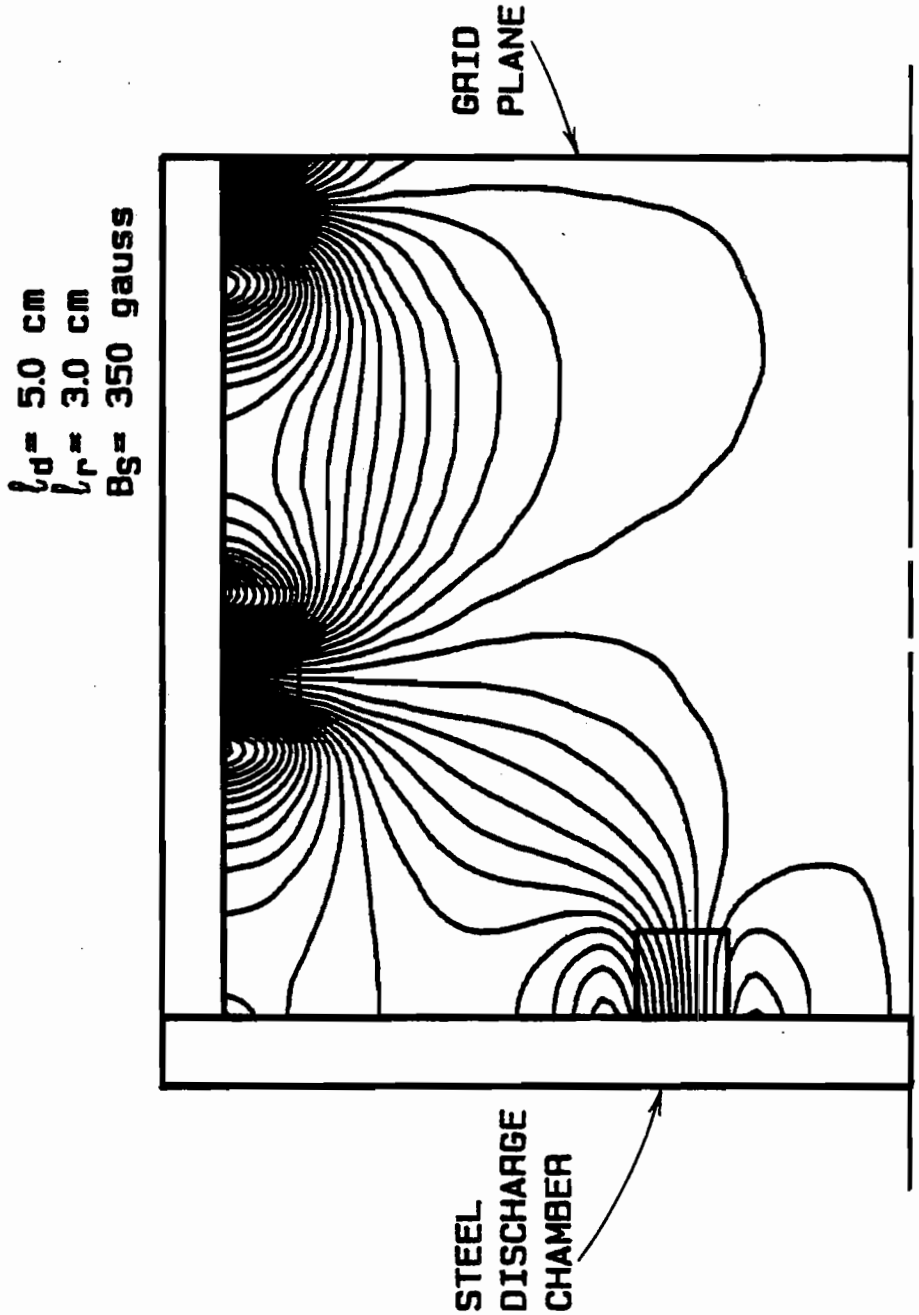

Fig. 18 Pseudo Iron Filings Map (B_S= 350 gauss)

the walls becomes small compared to the relatively magnetic flux independent ion loss rate through the cusps.

Figure 19 presents magnetic flux density contour maps for the two extreme magnetic flux density conditions considered in this study, which illustrate why extracted ion fractions are greater at the high flux density than they are at the low flux density. Increasing the surface flux density (B_S) from 350 to 2700 gauss is seen to increase the flux density throughout the chamber. Because the Bohm diffusion coefficient varies inversely with flux density, electron and ion flow across field lines to the anode and to the chamber wall will therefore be substantially less in the high flux density case.

Magnetic Field Configuration

Tests to investigate the effect of axial movement of the centrally located ring magnet were conducted by varying the position this magnet ring (ℓ_r in Fig. 3) measured with respect to the screen grid. In this study the central ring magnet was moved axially from 2.7 cm to 3.6 cm in order to induce some degree of change in the discharge chamber performance parameters. The effects of increasing ℓ_r from 2.7 cm to 3.6 cm (i.e. moving the ring magnet upstream towards the rear of the discharge chamber) on the discharge chamber performance parameters (ϵ_P^*, C_0 and f_B) are shown in Fig. 20. These particular data were recorded with the anode and cathode positions (ℓ_a and ℓ_c in Fig. 3) held constant relative to the ring magnet being moved (i.e. ℓ_r, ℓ_c and ℓ_a were moved in unison). The tests were conducted using a ring magnet surface flux density of 1200 gauss because lesser values yielded poor

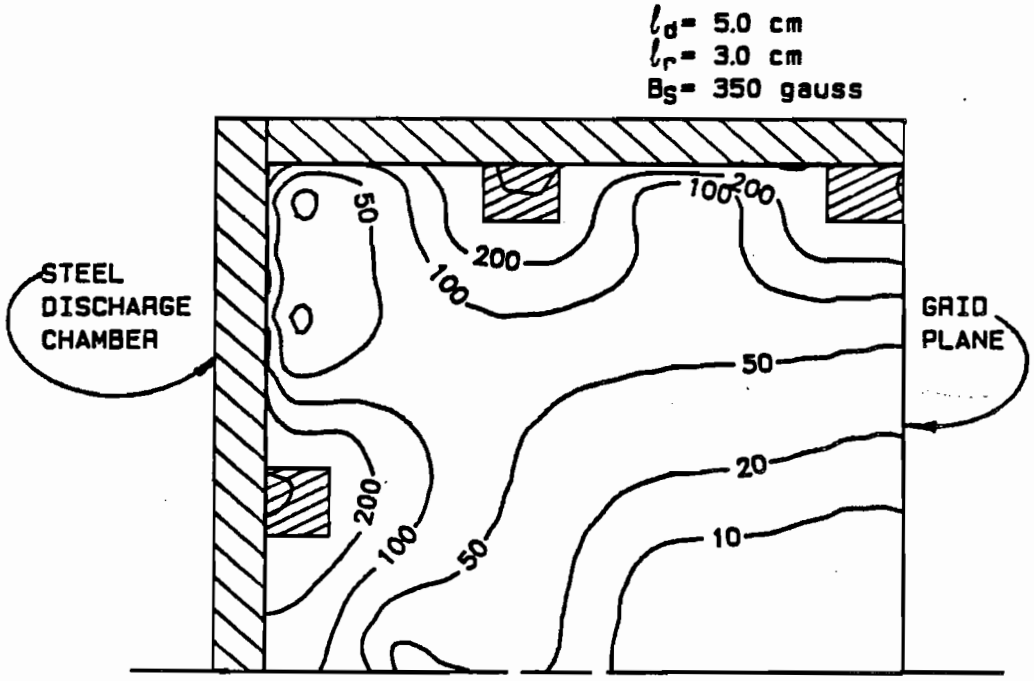

Fig. 19a Magnetic Flux Density Contour Maps
(350 gauss Surface Flux Density)

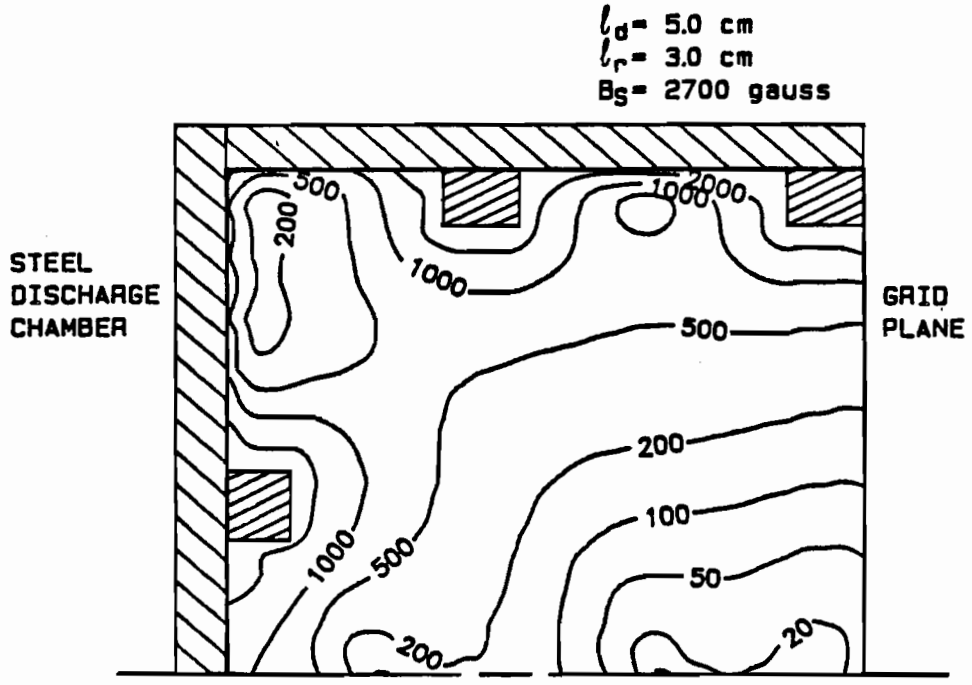

Fig. 19b Magnetic Flux Density Contour Map
(2700 gauss Surface Flux Density)

performance parameters (Fig. 17) and higher values tended to reduce the volume of the low magnetic flux density region in the chamber (Fig. 19b).

The results of this test presented in Fig. 20 show that the movement of the ring magnet upstream induces 1) a minimum rate of Maxwellian electron collection at ℓ_r= 3.0 cm (ϵ_p^* is a minimum), 2) a minimum rate of primary electron collection at ℓ_r= 3.0 cm (C_0 is a maximum) and 3) an increase in ion collection to the discharge chamber surfaces (f_B decreases). When all the performance data are taken into account (i.e. the values of ϵ_p^*, C_0 and f_B) the best performance for the discharge chamber with the dimensions identified in the legend (see Fig. 3) occurs when the ring magnet is positioned at ℓ_r= 3.0 cm where the primary and Maxwellian electron losses to the anode and ion loss to the discharge chamber surfaces is low. If the ring magnet is moved further upstream, the inefficient containment of the electrons and ions degrades discharge chamber performance.

The reason the extracted ion fraction decreases when the ring cusp is moved upstream to a position 3.6 cm from the grid plane can be seen by comparing the flux density contour maps shown in Fig. 21. The two maps shown in Figs. 21a and 21b were made with the ring magnet positioned at ℓ_r= 3.0 and 3.6 cm, respectively. This comparison shows the magnetic flux density gradient near the discharge chamber wall between the two radially facing ring magnets increases as the central magnet is moved upstream. This occurs because increasing numbers of field lines go to the iron side wall rather than to the adjacent, opposite polarity magnet as they are moved apart. This increased flux

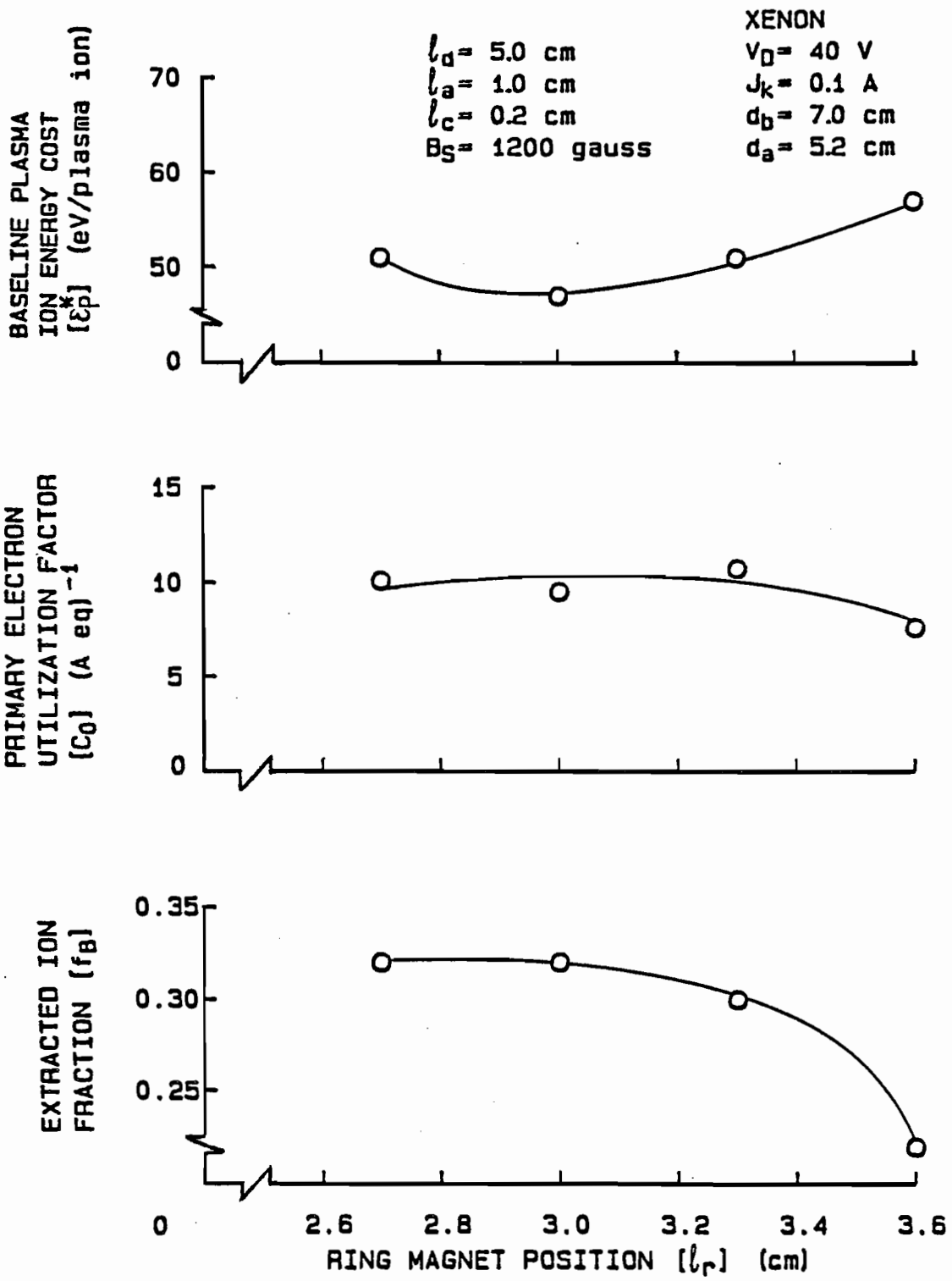

Fig. 20 Effect of Ring Magnet Position on Discharge Chamber Performance Parameters

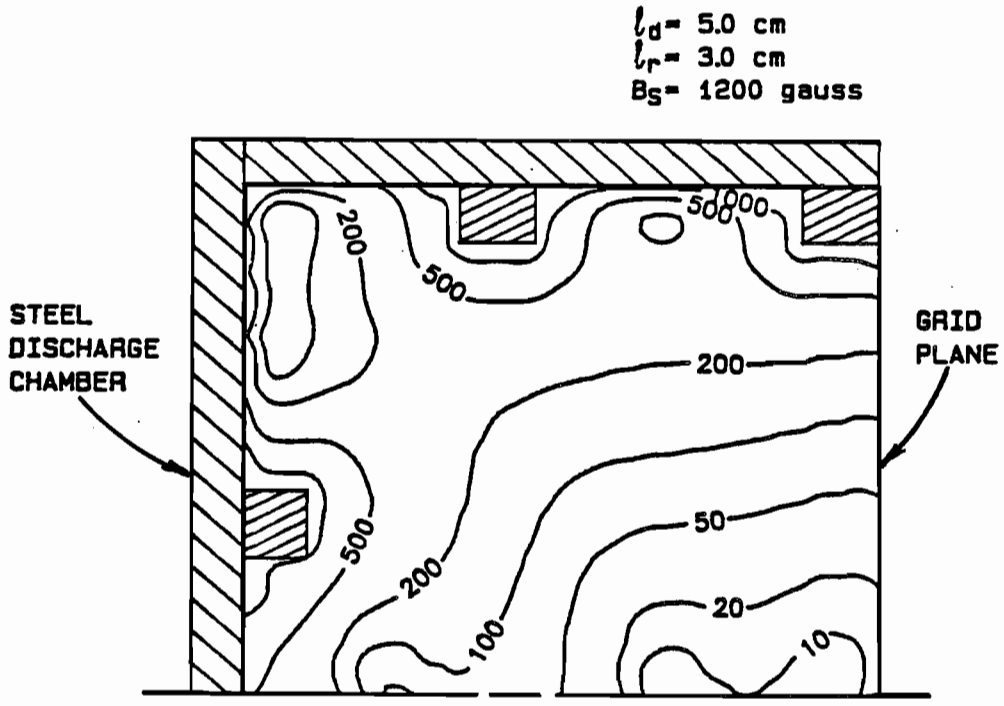

Fig. 21a Magnetic Flux Density Contour Map (ℓ_r = 3.0 cm)

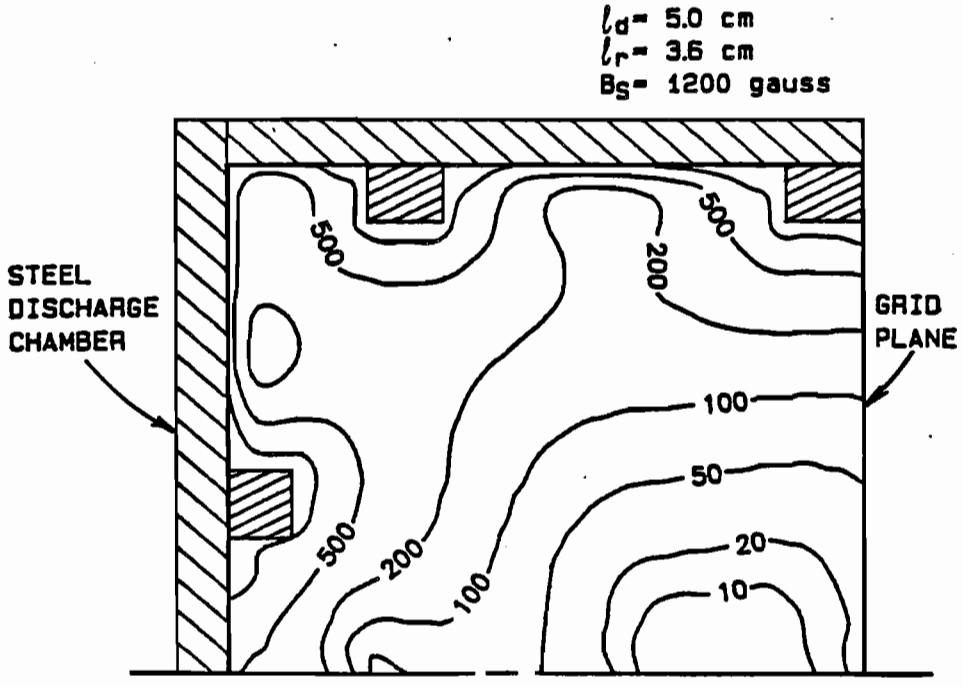

Fig. 21b Magnetic Flux Density Contour Map (ℓ_r = 3.6 cm)

density gradient caused by increasing ℓ_r causes the measured ion current going to the discharge chamber wall to increase and the extracted ion fraction shown in Fig. 20 to decrease.

During the test just described the beam flatness parameter increased in the manner shown in Fig. 22 as the ring magnet was moved upstream. The beam flatness parameter (the average-to-peak beam current density ratio) provides an indirect indication of the fraction of the screen grid being exposed to the discharge chamber plasma. This result occurs because more of the screen grid is exposed to uniform density discharge chamber plasma as the ring magnet position is moved further upstream. This occurs because the primary plasma volume, which is the volume of the chamber that the primary electrons occupy where the bulk of the ionization takes place, inside the discharge chamber increases, and as a result the grid system is being used more effectively; that is less unionized propellant is being lost through the grids (a fact that was also confirmed by independent propellant utilization efficiency measurements). This result when considered with the extracted ion fraction data (f_B-- lower plot of Fig. 20) shows that increasing the primary plasma volume is beneficial because of the increased propellant utilization efficiency, but if the magnetic field strength near the discharge chamber walls is not sufficient to prevent ion losses through Bohm diffusion then the increased plasma volume enhances ion losses and decreases performance.

In order to produce a magnetic field configuration that would produce good discharge chamber performance and a flat ion beam, the magnetic flux density near the wall should be large enough to prevent ion losses through Bohm diffusion, yet allow the primary discharge chamber plasma to occupy a large fraction of the discharge chamber

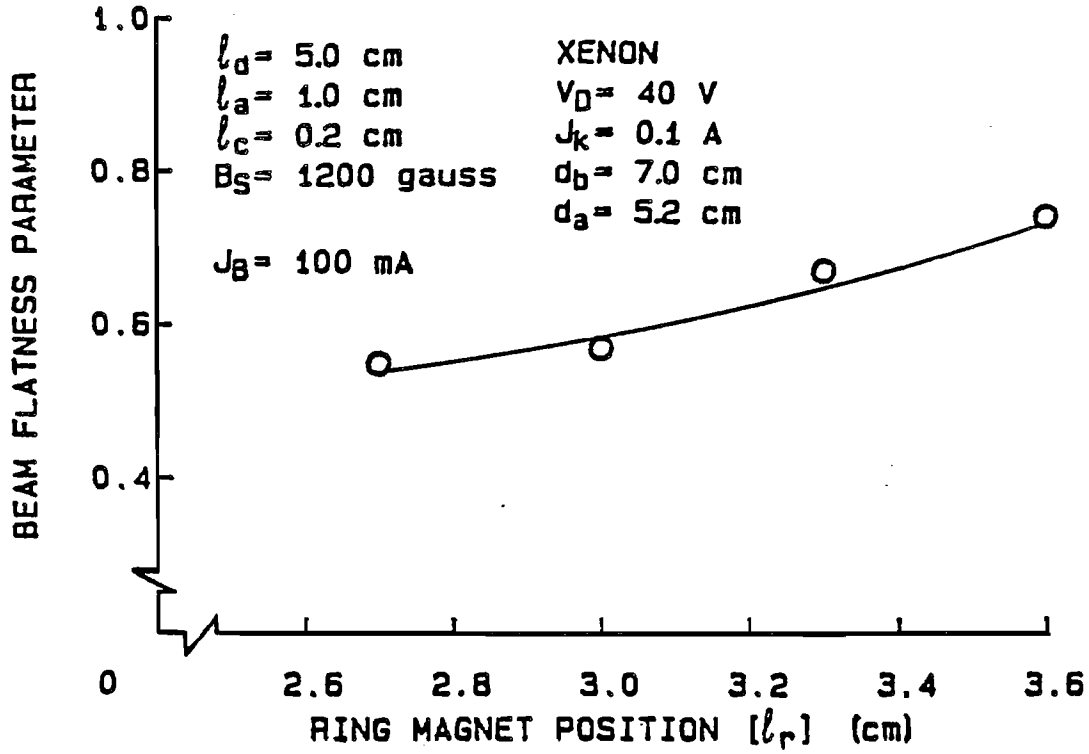

Fig. 22 Effect of Ring Magnet Position on Beam Flatness Parameter

volume adjacent to the grids. In the study conducted by Hiatt [1] with a filament cathode in a small diameter discharge chamber, this condition was approached by using a high flux density ring magnet (~2700 gauss) and setting the diameter of the annular zone of electron emission from the cathode to a substantial fraction of the source diameter. This made it possible to achieve relatively high primary electron (and therefore plasma) densities over a rather large volume in the discharge chamber and still limit ion diffusion to the chamber walls. However, for the present study where a hollow cathode was being used the point of electron injection remained on the chamber centerline and the magnetic field was altered by reducing the ring magnet strength so the volume occupied by the primary plasma could expand. Based on the observations of these tests it also enhanced the rate of ion diffusion to the chamber walls. It is argued, that the simultaneous requirement for a substantial primary electron plasma volume to exist near the outer edge of the screen grid and for small magnetic flux density gradients to exist near the chamber walls to prevent ion diffusion losses cannot be achieved in a small diameter chamber with the cathode on the centerline.

V. CONCLUSIONS

By examining the effects of changes in hollow cathode discharge chamber performance parameters (ϵ_P^*, C_0, and f_B) induced by changes in discharge chamber dimensions and magnetic field strengths it is possible to examine specific physical phenomena that induce changes in discharge chamber performance. This technique has been used to identify the effects induced by changes in anode and hollow cathode position and magnetic field strength and geometry on the performance of a small diameter discharge chamber.

Initial results obtained with a filament cathode positioned upstream of the cusp when the anode was on the cusp show that discharge chamber performance improves as the diameter of the filament decreases. When a small diameter filament (2 mm) is used the performance of the discharge chamber is observed to be independent of upstream cathode position because the ion losses to the discharge chamber walls induced by Bohm diffusion do not change as the axial position of the cathode is changed.

The performance of a discharge chamber which utilizes either a hollow cathode or a refractory filament (diameter of 2 mm) is similar provided the cost of operating the hollow cathode is taken into account in plasma ion energy cost calculations. Because these two cathodes have been shown to exhibit similar discharge chamber performance, it is argued that movement of a hollow cathode along the discharge chamber centerline should be similar to that observed when the upstream

filament cathode is moved axially. When the hollow cathode is moved along the chamber centerline the extracted ion fraction and baseline plasma ion energy cost change in such a way that their combined effect on performance is almost nil provided the cathode is not moved upstream of the point of peak centerline magnetic flux density. Movement upstream of this point of peak magnetic flux density causes a rapid degradation in performance as a result of ion recombination on hollow cathode surfaces.

Moving the point of primary electron injection into the plasma off of the discharge chamber centerline improves performance by increasing the volume of the region in which primary electrons can ionize neutral atoms. However, increases in the primary plasma volume that are not accompanied by movement of the anode further from the field line onto which electrons are injected and adjustment of magnet rings to close zones of high flux density gradient at the walls can cause direct loss of primary and high energy Maxwellian electrons to the anode and ions to discharge chamber surfaces.

Results obtained with the anode positioned downstream of a ring cusp in a hollow cathode equipped discharge chamber are qualitatively similar to those obtained by Hiatt [1] using a discharge chamber with a similar beam diameter and a refractory filament cathode. Movement of the anode downstream of the ring cusp toward the grids reduced the primary electron losses to the anode and caused the primary electron utilization factor C_0 to increase continuously up to the point where the discharge impedance becomes so great that significant discharge currents could no longer be drawn without increasing the discharge voltage.

An increase in the surface flux density of the ring magnets improves the confinement of both primary electrons and ions up to a surface flux density of ~1200 gauss. Increases in surface flux density beyond this value induce negligible additional improvement in the confinement of each species. Upstream movement of the central ring magnet in the discharge chamber introduces competing performance effects. It causes the volume of the ionizing plasma adjacent to the grids to increase while at the same time allowing increased ion losses to the discharge chamber walls in the region between the downstream and central magnet rings.

REFERENCES

1. Hiatt, J. M. and Wilbur, P. J., "Ring Cusp Discharge Chamber Performance Optimization," Journal of Propulsion and Power, Vol. 2, No. 5, Sept.-Oct. 1986, pp. 390-397.

2. Sovey, J. S., "Improved Ion Containment Using a Ring-Cusp Ion Thruster," AIAA Paper 82-1928, Nov. 1982.

3. Siegfried, D. E., "A Phenomenological Model for Orificed Hollow Cathodes," NASA CR-168026, December, 1982.

4. Holt, E. H. and Haskell, R. E., Foundations of Plasma Dynamics, The Macmillan Company, New York, 1965, pp. 187-90.

5. Brophy, J. R., "Ion Thruster Performance Model," NASA CR-174810, December, 1984.

6. Vaughn, J. A., "8 cm Dia. Ring Cusp Discharge Chamber Research," appears in "Advanced Electric Propulsion Research," NASA CR-182130, P. J. Wilbur, ed., pp. 1-52, Jan. 1988.

7. Huddlestone, R. H. and Leonard, S. L., Plasma Diagnostic Techniques, Academic Press, New York, 1965, pp. 537-40.

8. Wilbur, P. J., "A technique for Making Iron Filings Maps in Strong Field from Permanent Magnets," appears in "Advanced Ion Thruster Research," NASA CR-174862, Jan. 1985.

9. Arakawa, Y. and Wilbur, P. J., "Discharge Plasma Calculations in Cusped Ion Thrusters Using the Finite Element Method," IEPC 88-079, 20th International Electric Propulsion Conference, Garmisch-Partenkirchen, West Germany, Oct. 3-6, 1988.

10. Vaughn J. A. and Wilbur P. J.,"Hollow Cathode/Ring Cusp Discharge Chamber Performance Studies", IEPC 88-064, 20th International Electric Propulsion Conference, Garmisch-Partenkirchen, West Germany, Oct. 3-6, 1988.

APPENDIX A

THE EFFECTS OF ION LOSSES TO CATHODE OR ANODE SURFACES ON DISCHARGE CHAMBER PERFORMANCE PARAMETERS

When ions produced in a discharge chamber are lost to an anode or cathode surface, they cannot be measured because they cannot be distinguished from electrons that must flow to and from these surfaces to sustain the plasma discharge. Because of this a discharge chamber alteration that causes ions, which had been going to a chamber wall where they could be measured, to go instead to a cathode or anode surface would cause an apparent increase in both the extracted ion fraction f_B and the baseline plasma ion energy cost ϵ_p^*. In order to establish a relationship between the apparent and true values of these parameters the following definitions are offered:

$\hat{\epsilon}_p$ • The true plasma ion energy cost (based on all ions produced whether they can be measured or not),

ϵ_p • The apparent or measured plasma ion energy cost (based only on the ion currents going to surfaces where measurements can be made),

J_B, J_W, J_S • Measured beam current, wall current, and screen current, respectively,

J_L • Ion loss current that cannot be measured (i.e. going to a cathode or anode surface),

$\hat{f}_B$ • The true extracted ion fraction (based on all ions produced),

f_B • The apparent or measured extracted ion fraction (based only on the ion current that can be measured).

Since the power being used to create the plasma ions is the same regardless of the accounting scheme used one can write

$$P = (J_B + J_S + J_W)\ \epsilon_P = (J_B + J_S + J_W + J_L)\ \hat{\epsilon}_P. \qquad (A1)$$

Further, the true and apparent extracted ion fractions are given by:

$$\hat{f}_B = \frac{J_B}{(J_B + J_S + J_W + J_L)} \qquad (A2)$$

and

$$f_B = \frac{J_B}{(J_B + J_S + J_W)}\ . \qquad (A3)$$

Combining Eqs. A1, A2 and A3 to eliminate the currents one obtains

$$\frac{\hat{\epsilon}_P}{\epsilon_P} = \frac{\hat{f}_B}{f_B} \qquad \text{(A4)}$$

This equation can be written in terms of the baseline plasma ion energy cost (ϵ_P^*) using Eq. 5 and since the primary electron utilization factor C_0 is not affected by ion losses to the anode or cathode (see Fig. 14), the resulting equation can be simplified further to obtain

$$f_B = \frac{\hat{f}_B}{\hat{\epsilon}_P^*} \epsilon_P^* \ . \qquad \text{(A5)}$$

Hence plasma ion losses to anode or cathode surfaces will induce increases in apparent extracted ion fraction and apparent baseline plasma ion energy cost that are proportional to each other.